Article

Cell Reports

hESC-Derived Dopaminergic Transplants Integrate into Basal Ganglia Circuitry in a Preclinical Model of Parkinson's Disease

Graphical Abstract

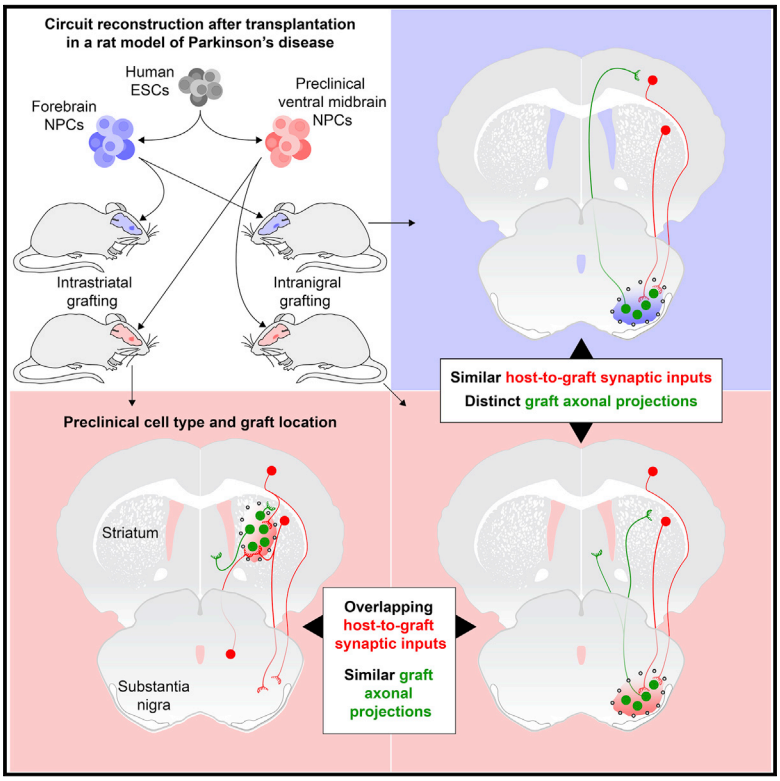

Highlights

- Pattern of graft-derived innervation is determined by phenotype of grafted cells
- Synaptic inputs from host-to-graft depend on location of graft
- Intrastriatal dopaminergic grafts receive correct excitatory and inhibitory host inputs
- Individual host neurons provide inputs to both dopaminergic grafts and the host nigra

Authors

Andrew F. Adler, Tiago Cardoso, Sara Nolbrant, ..., Shane Grealish, Anders Björklund, Malin Parmar

Correspondence

malin.parmar@med.lu.se

In Brief

Adler et al. graft hESC-derived dopaminergic progenitors into a rat model of Parkinson's disease. They find grafts correctly innervate host targets and receive appropriate synaptic input after intranigral and intrastriatal placement. Furthermore, the same host neurons projecting toward endogenous dopamine neurons are found to also connect to the grafts.

Adler et al., 2019, Cell Reports *28*, 3462–3473
September 24, 2019
https://doi.org/10.1016/j.celrep.2019.08.058

CellPress

OPEN ACCESS
CellPress

Cell Reports
Article

hESC-Derived Dopaminergic Transplants Integrate into Basal Ganglia Circuitry in a Preclinical Model of Parkinson's Disease

Andrew F. Adler,[1,2,3] Tiago Cardoso,[1,2,3] Sara Nolbrant,[1,2] Bengt Mattsson,[1] Deirdre B. Hoban,[1,2] Ulla Jarl,[1] Jenny Nelander Wahlestedt,[1,2] Shane Grealish,[1] Anders Björklund,[1] and Malin Parmar[1,2,4,*]

[1]Developmental and Regenerative Neurobiology, Department of Experimental Medical Science, Wallenberg Neuroscience Center, Lund University, 22184 Lund, Sweden

[2]Lund Stem Cell Center, Lund University, 22184 Lund, Sweden

[3]These authors contributed equally

[4]Lead Contact

*Correspondence: malin.parmar@med.lu.se

https://doi.org/10.1016/j.celrep.2019.08.058

SUMMARY

Cell replacement is currently being explored as a therapeutic approach for neurodegenerative disease. Using stem cells as a source, transplantable progenitors can now be generated under conditions compliant with clinical application in patients. In this study, we elucidate factors controlling target-appropriate innervation and circuitry integration of human embryonic stem cell (hESC)-derived grafts after transplantation to the adult brain. We show that cell-intrinsic factors determine graft-derived axonal innervation, whereas synaptic inputs from host neurons primarily reflect the graft location. Furthermore, we provide evidence that hESC-derived dopaminergic grafts transplanted in a long-term preclinical rat model of Parkinson's disease (PD) receive synaptic input from subtypes of host cortical, striatal, and pallidal neurons that are known to regulate the function of endogenous nigral dopamine neurons. This refined understanding of how graft neurons integrate with host circuitry will be important for the design of clinical stem-cell-based replacement therapies for PD, as well as for other neurodegenerative diseases.

INTRODUCTION

The adult human brain has a limited capacity for repair, and new neurons are not normally generated after injury and disease. Cell replacement by transplantation of fetal cells has been developed as a therapeutic strategy aimed to replace neurons lost in neurodegenerative disorders such as Parkinson's and Huntington's disease (Bachoud-Lévi, 2017; Barker et al., 2013, 2017), as well as in retinal degenerative disorders (Shirai et al., 2016; Whiting et al., 2015) and stroke (Kalladka et al., 2016; Lindvall and Kokaia, 2011). Parkinson's disease (PD) has been a primary target for cell replacement therapy by using intrastriatal transplants of fetal dopamine (DA) neurons and is also the first neurodegenerative disease where translational work using pluripotent stem-cell-derived DA neurons has reached the point of clinical trial (Barker et al., 2017; Kirkeby et al., 2017; Studer, 2017; Takahashi, 2017). A number of studies have shown that transplanted fetal- and stem-cell-derived DA neurons are phenotypically similar and that they survive, innervate, and function with equal potency after transplantation in preclinical models of PD (Grealish et al., 2014; Kikuchi et al., 2017; Kriks et al., 2011). New chemo- and optogenetic technologies enabling the specific activation and inhibition of graft-derived neurons have also provided a deeper understanding of transplant function in animal models of PD (Aldrin-Kirk et al., 2016; Chen et al., 2016; Steinbeck et al., 2015).

In previous studies, we have used graft-initiated monosynaptic retrograde rabies virus tracing to map the extent of host-to-graft connectivity (Cardoso et al., 2018; Grealish et al., 2015; Tornero et al., 2017). These studies demonstrate that host neurons make abundant afferent synaptic contacts with the transplanted cells, providing evidence that the grafted human neurons can become functionally integrated into host circuitry. Still, little is known about what factors contribute to graft integration and the establishment of connections between host neurons and transplanted stem-cell-derived human neurons.

In this study, we have investigated the effects of grafted cell phenotype, graft location, and the extent of host DA depletion on the establishment of appropriately targeted graft-derived axonal projections and monosynaptic inputs from host neurons onto grafted cells, in a long-term preclinical xenograft model of PD. We transplanted ventral midbrain (VM)-patterned human embryonic stem cells (hESCs) homotopically into the substantia nigra or ectopically into the striatum of adult 6-hydroxydopamine (6-OHDA)-lesioned immune-deficient or -suppressed rats. By comparing graft fiber innervation as well as afferent inputs from host neurons between each condition, and in comparison to ventral forebrain (FB)-patterned grafts devoid of mesencephalic DA neurons, we demonstrate that the capacity for graft fibers to innervate correct target structures is regulated by cell-intrinsic factors as previously shown (Hargus et al., 2010; Isacson and Deacon, 1996; Michelsen et al., 2015; Niclis et al.,

2017), whereas host-to-graft synaptic integration is largely determined by graft placement, as has been observed for hESC-derived GABAergic transplants (Doerr et al., 2017).

In the clinical trials conducted to date using fetal cells, VM cells have been grafted ectopically into the caudate and putamen to decrease the distance that DA axons must grow from the graft to reach targets relevant to motor function in the striatum (Barker et al., 2013). Despite the ectopic location of DA neurons in the host brain, a functional and appropriately regulated release of DA seems to be achieved in patients (Barker et al., 2013; Kefalopoulou et al., 2014). This is also the case in preclinical experimental animal models where the cells are commonly placed ectopically in the FB (Fisher et al., 1991; Piccini et al., 1999; Sørensen et al., 2005; Steinbeck et al., 2015). In this study, we compared host inputs to the graft when the stem-cell-derived dopaminergic transplants were placed ectopically in the striatum, mimicking the clinical scenario, with host inputs to the graft when the cells were placed homotopically in the midbrain. We found grafts placed in the striatum receive afferent input from the same subtypes of host cortical, striatal, and pallidal neurons, which are known to regulate the function of endogenous nigral DA neurons. By combining two types of retrograde tracers, we further show that individual host neurons located in these regions provide input to both the transplanted neurons and to endogenous neurons in the substantia nigra, simultaneously. We also show the extent of DA depletion does not affect the overall extent or origin of host to graft connectivity but that it alters the ratio of input from host structures to the transplanted cells. The observed ability of intrastriatal hESC-derived dopaminergic grafts to appropriately integrate into basal ganglia circuitry, despite their ectopic placement, rationalizes their ability to release DA in a functionally appropriate and clinically efficacious manner.

RESULTS

Target-Specific Fiber Outgrowth from Transplanted hESC-Derived Neurons Is Determined by Cell Phenotype

Rodent, porcine, and human mesencephalic dopaminergic grafts of fetal or pluripotent stem cell origins have the capacity to extend axons long distances to innervate appropriate FB targets when placed in the rodent substantia nigra (Cardoso et al., 2018; Gaillard et al., 2009; Grealish et al., 2014; Isacson et al., 1995; Thompson et al., 2009; Wictorin et al., 1992). Furthermore, dopaminergic grafts placed ectopically into the striatum also innervate functionally appropriate host target regions (Grealish et al., 2010, 2014; Hargus et al., 2010; Niclis et al., 2017; Thompson et al., 2005), and the specificity of human and porcine graft axonal outgrowth upon ectopic and homotopic placement is maintained in rat xenograft models (Isacson and Deacon, 1996; Wictorin et al., 1992). Thus, targeted axonal outgrowth is an established hallmark of functional dopaminergic grafts (Hargus et al., 2010; Niclis et al., 2017) and, as such, is an important component of preclinical validation. To address this with our preclinical cell source, we patterned hESC-derived neural progenitors toward a VM fate or ventral FB fate *in vitro*. This comparison was designed to determine if the specificity of innervation of DA targets depends on the midbrain identity of the cells, as has been reported previously, or if it is primarily due to graft placement in the nigrostriatal pathway, along which the endogenous host midbrain neurons normally project toward their appropriate FB targets. The regional identities of the cell preparations were assessed using a panel of markers to document their correct patterning (Figures S1A–S1D) and subsequently transplanted to the nigra or striatum of rats with unilateral 6-OHDA lesions to the medial forebrain bundle (MFB). Before grafting, the cells were transduced *in vitro* with a lentiviral rabies tracing construct expressing nuclear GFP as well as the components necessary for monosynaptic rabies tracing (discussed in the next section). Six months after transplantation, both the VM- and FB-patterned progenitors matured into neuron-rich grafts of similar sizes, as assessed by staining for the human neural cell adhesion molecule (hNCAM) (Figures 1A and 1G). Tyrosine hydroxylase (TH) (Figures 1B and 1H) and FOXA2 (Figures 1C and 1I) were co-expressed exclusively in VM-patterned grafts, confirming that only the VM-patterned progenitors had the capacity to mature into midbrain DA neurons *in vivo*. In contrast, many of the cells in the FB- but not VM-patterned grafts expressed NKX2.1 and FOXG1 (Figures 1D, 1E, 1J, and 1K), indicating they adopted a ventral FB identity. These FB-patterned grafts also contained DARPP-32$^+$ neurons (Figures 1F and 1L).

An analysis of graft-derived innervation patterns, compiled from all animals, confirmed that axonal projections from VM-patterned grafts placed in the nigra extended along trajectories that closely mimicked the intrinsic nigrostriatal and mesolimbocortical pathways and innervated appropriate dopaminergic neuron target areas in the FB, including the dorsolateral striatum (dlSTR), nucleus accumbens (NAcc), and ventromedial prefrontal cortex (PFC) (Figures 2A and 2C), with little if any innervation of the insular cortex (Figure 2D). From the FB-patterned intranigral grafts, hNCAM$^+$ fibers could also be seen coursing rostrally by the MFB to innervate FB target areas (Figure 2B). However, in marked contrast to the VM-patterned grafts, the FB-patterned cells preferentially innervated more dorsal and lateral cortical areas, such as motor and insular cortex (INS) (Figures 2B and 2F) and did not innervate A9 dopaminergic target areas, such as the dlSTR (Figures 2B and 2E). Thus, despite being placed in the same anatomical location and initially extending axons rostrally along the same trajectory, intranigral VM- and FB-patterned transplants innervated distinct and appropriate host target structures (quantified in Figure 2J), confirming that the innervation was determined by cell phenotype. This was further substantiated by tissue clearing and light sheet microscopy to provide an overview of the outgrowth of TH$^+$ fibers from VM-patterned grafts placed in the nigra after 16 weeks of maturation (Figure 2I; Videos S1 and S2). After 24 weeks of maturation, VM- but not FB-patterned grafts placed in the nigra reinnervated the DA-depleted striatum with a significant number of graft-derived TH$^+$ fibers (Figures 2G, 2H, and 2K).

In a parallel set of experiments where the same cell preparations were transplanted to the striatum, we observed VM- and FB-patterned grafts reaching similar targets as when placed in the nigra, with a bias for hypothalamic and cortical innervation from VM- and FB-patterned grafts, respectively (Figures 3A–3F, quantified in 3L). Also, we confirmed the dopaminergic phenotype of graft-derived fibers from VM- but not FB-patterned

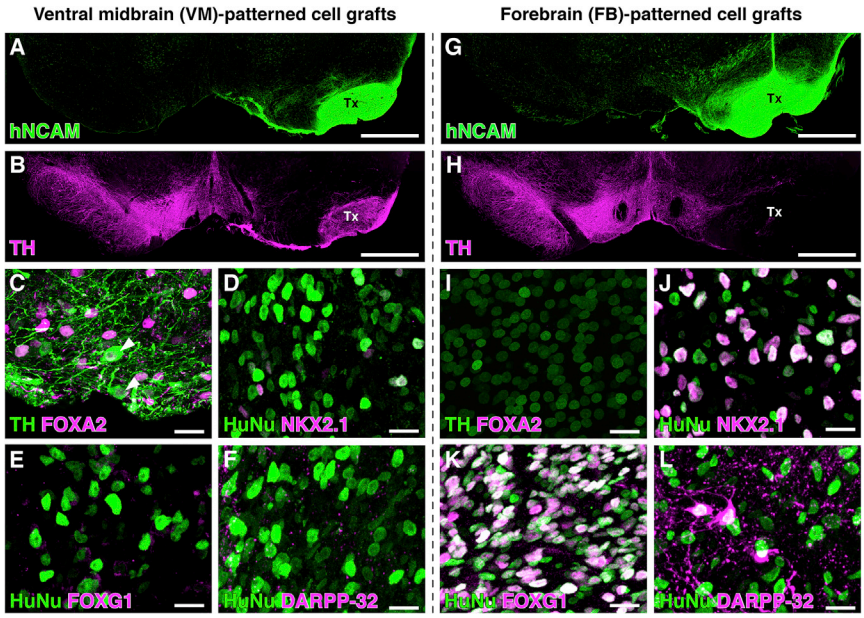

Figure 1. Comparison of VM- versus FB-Patterned Graft Composition

Phenotypic characterization of hESC-derived VM-patterned (A–F) and FB-patterned cells (G–L) 6 months after grafting to the nigra.

(A, B, G, and H) VM- (A) and FB-patterned cells (G) generated grafts of comparable size, as visualized by human NCAM staining. VM- (B) but not FB-patterned grafts (H) generated TH^+ neurons *in vivo*.

(C and I) In VM-patterned grafts (C) but not FB-patterned grafts (I), TH^+ neurons also co-expressed the midbrain DA neuron marker FOXA2 (arrowheads).

(D–F and J–L) FB- (J) but not VM-patterned graft cells ($HuNu^+$) (D) expressed NKX2.1 and FOXG1 (E and K), and included DARPP-32^+ neurons (F and L). See also Figure S1 for *in vitro* characterization of cell preparations.

All graft neurons expressed a rabies tracing construct and, thus, nuclear GFP. Scale bars represent 1 mm (A, B, G, and H) and 20 μm (C–F and I–L). Images in (A), (B), (G), and (H) are digitally stitched from multiple high-magnification images. DARPP-32, dopamine- and cAMP-regulated phosphoprotein; FB, forebrain; FOXA2, forkhead box A2; FOXG1, forkhead box protein G1; hESCs, human embryonic stem cells; HuNu, human nucleus; NKX2.1, NK2 homeobox 1; TH, tyrosine hydroxylase; Tx, transplant; VM, ventral midbrain.

grafts (Figures 3G–3I; Video S3). In the reinnervated striatum, the graft-derived TH^+ fiber density was below that of the intact contralateral striatum (Figures 3J and 3K) but is commensurate with the extent of reinnervation required for functional recovery (Cardoso et al., 2018). Taken together, these results further support that consistent patterns of targeted innervation were largely determined by cell-intrinsic factors, rather than by graft location or proximity to the lesioned MFB.

The Anatomical Origins of Monosynaptic Host Inputs to Transplanted Neurons Are Not Strongly Influenced by Cell Phenotype

We next mapped host-to-graft synaptic connectivity 6 months after transplantation of VM- and FB-patterned grafts placed in the substantia nigra in 6-OHDA-lesioned rats by using monosynaptic tracing with envelope glycoprotein of the subgroup A avian sarcoma leucosis virus (EnvA)-pseudotyped glycoprotein-deleted (ΔG) rabies virus (Wickersham et al., 2007). In this system, primary infection and monosynaptic spread from grafts strictly depend on ectopic expression of the subgroup A avian sarcoma leucosis virus (TVA) receptor and rabies glycoprotein, respectively, which are expressed in the cells prior to grafting by transduction with a lentiviral helper construct *in vitro*. The batch of mCherry EnvA-pseudotyped ΔG-rabies we used in this study has been validated to spread transsynaptically only in the presence of glycoprotein (Grealish et al., 2015), and in this study, we again confirmed that tracing was only initiated by grafts expressing the TVA receptor (Figure S2A). When quantifying the number of starter cells, we found that approximately 40% of VM-patterned starter neurons expressed TH (Figures S2B and 2C). For both VM- and FB-patterned intranigral grafts, we observed a similar pattern of inputs from host neurons located in the striatum, sensorimotor cortex, pallidum, and amygdala (Figures 4A–4F, 4M, and 4N), which are the principal FB structures that normally provide input to neurons in the intact VM (Cardoso et al., 2018; Watabe-Uchida et al., 2012), as well as from hypothalamic and midbrain raphe nuclei (Figures 4M and 4N). Interestingly, the anatomical origins of host inputs to the FB-patterned grafts (Figures 4B and 4N) were not significantly different from those contacting VM-patterned grafts (Figures 4A and 4M). This suggests that the phenotype of the cells grafted and the presence of dopaminergic neurons have a limited impact on the identity of host input structures.

The Anatomical Origins of Monosynaptic Host Inputs to Transplanted Neurons Are Influenced by Graft Placement

To further investigate factors controlling afferent connectivity after transplantation, we mapped the pattern of host neurons making monosynaptic contact with VM- and FB-patterned cells transplanted to either the striatum or the substantia nigra of DA-depleted athymic nude rats. When directly comparing host inputs to the VM-patterned cells grafted in the nigra with those grafted to the striatum (compare Figures 4A and 4G), we found that they received afferent input from different host regions depending on graft placement. In contrast to what we observed for intranigral grafts, host neurons that connected with intrastriatal graft neurons were located in structures that normally innervate, or send axons of passage through, the striatum.

Closer analysis, however, including quantification of the inputs to VM-patterned grafts placed in the nigra compared to the same cells placed in the striatum, revealed that the origin of monosynaptic inputs to VM-patterned intrastriatal grafts (Figures 4G, 4I, 4J, and 4M) partially overlapped with inputs to

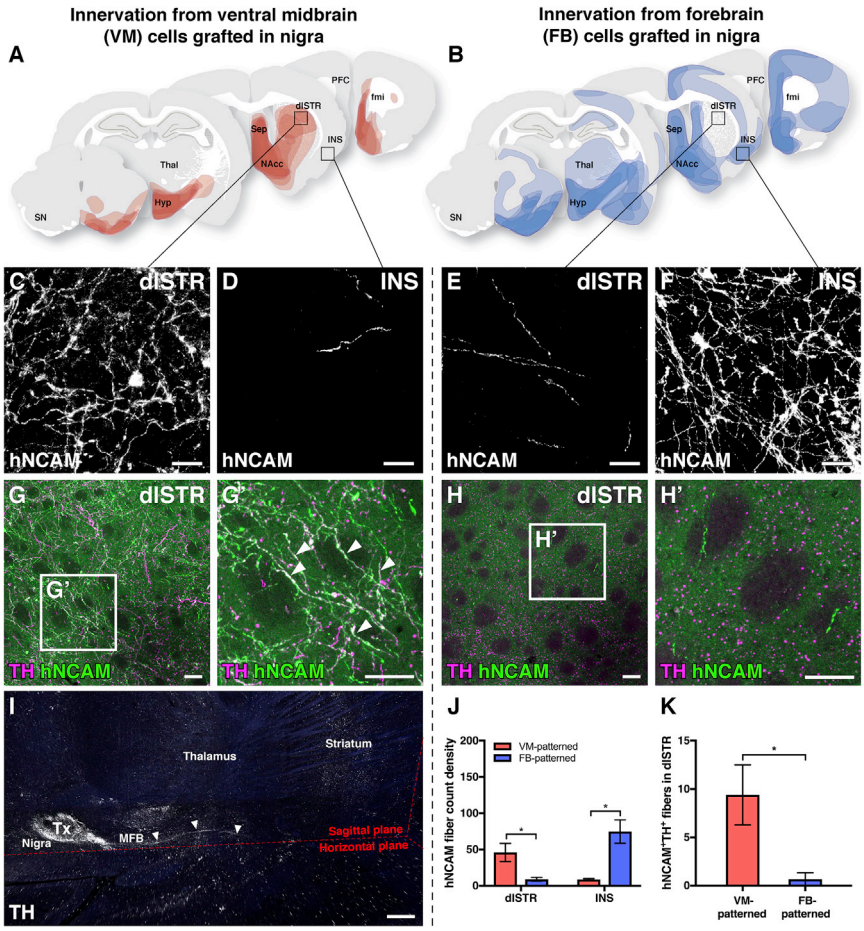

Figure 2. Comparison of Fiber Outgrowth from VM- versus FB-Patterned Grafts Placed into the Substantia Nigra

(A and B) Figures showing composite data of graft-derived innervation of host structures as detected by DAB-developed hNCAM staining for grafts placed in the nigra of 6-OHDA lesioned rats after 24 weeks of graft maturation (combines and visualizes data collected from n = 5 animals in A and n = 6 animals in B). Data from the group of animals in (A) have also been used in Cardoso et al., 2018.

(C–F) VM-patterned neurons targeted fiber outgrowth toward dorsolateral striatum (dlSTR) (C) but not insular cortex (INS) (D), while FB-patterned neurons extensively INS (F) but not dlSTR (E).

(G) Human (hNCAM$^+$) TH$^+$ fibers reinnervated the dopamine-depleted striatum from VM-patterned grafts.

(H) Comparatively sparse TH$^-$ fibers extended into the striatum from FB-patterned grafts.

(I) Tissue clearing and light sheet microscopy provides an overview of graft-derived TH$^+$ fibers extending to reinnervate the DA-depleted host striatum after 16 weeks of maturation, with endogenous autofluorescence shown in blue (see associated Videos S1 and S2).

(J and K) Quantitative image analysis of hNCAM$^+$ (J) and hNCAM$^+$TH$^+$ (K) fiber outgrowth confirms that 24-week VM-patterned grafts preferentially innervated the dlSTR, whereas FB-patterned grafts preferentially innervated insular cortex (VM cells, n = 5 animals; FB cells, n = 6 animals; mean ± SEM, $p < 0.05$, $\alpha = 0.05$, two-way ANOVA with Bonferroni-corrected post hoc testing for hNCAM, unpaired two-tailed t test for hNCAM$^+$TH$^+$).

Scale bars represent 20 μm (C–F), 50 μm (G and H), and 500 μm (I, sagittal plane). 6-OHDA, 6-hydroxydopamine; DAB, 3,3′-diaminobenzidine; dlSTR, dorsolateral striatum; fmi, forceps minor; FB, forebrain; hNCAM, human neural cell adhesion molecule; Hyp, hypothalamus; INS, insular cortex; MFB, medial forebrain bundle; NAcc, nucleus accumbens; PFC, prefrontal cortex; Sep, septum; SN, substantia nigra; TH, tyrosine hydroxylase; Thal, thalamus; Tx, transplant; VM, ventral midbrain.

intranigral grafts of the same VM-patterned cells (Figures 4A, 4C, 4D, and 4M). For example, VM-patterned grafts in both locations received extensive inputs from sensorimotor cortex, striatum, and external globus pallidus (GPe) (Figures 4A, 4C, 4D, 4G, 4I, 4J, and 4M), which are principal FB regions involved in motor control (Gerfen, 1992; Shepherd, 2013). Transplants placed in the striatum received more abundant thalamic afferents but fewer inputs from hypothalamus and raphe (Figure 4M).

We observed a similar shift in the anatomical location of presynaptic host labeling when comparing inputs to FB-patterned grafts placed in the nigra (Figures 4B and 4N) versus FB-patterned grafts placed in the striatum (Figures 4H and 4N). The anatomical location of host neurons presynaptic to the intrastriatal grafts was not significantly altered by FB versus VM patterning (Figures 4M and 4N). Taken together, these results highlight the strong influence graft placement has on the anatomical origin of host afferent connectivity, which is in agreement with a previous comparison of hESC-derived GABAergic transplants placed either in the host hippocampus or striatum (Doerr et al., 2017).

VM-Patterned Grafts Placed in the Striatum Receive Monosynaptic Inputs from Functionally Appropriate Subtypes of Host Neurons

The human brain is much larger than the rodent brain, and to maximize the therapeutic effect of the transplant in PD patients, the cells are placed in FB target regions rather than in their endogenous midbrain location. This raises interesting questions relating to how graft function is mediated in the ectopic location. To investigate this, we performed a phenotypic analysis of major inputs to dopaminergic grafts placed in the midbrain or FB. We found that both intranigral (Figure 5A) and intrastriatal (Figure 5B) VM-patterned grafts received inputs from corticofugal neurons in the sensorimotor cortex (CTIP2$^+$ cortical neurons projecting to subcortical areas; (Molyneaux et al., 2007), as well as from mu-opioid-receptor-positive (MOR$^+$) medium spiny neurons (MSNs) in the striatum (Figures 5C and 5D), which normally project to the substantia nigra by the so-called direct pathway (Smith et al., 2016). In the GPe, we identified two subpopulations of neurons synapsing with intrastriatal VM grafts: parvalbumin-positive (PV$^+$) pallidal neurons (Figure 5F), marking a prototypic population with known collateral projections to

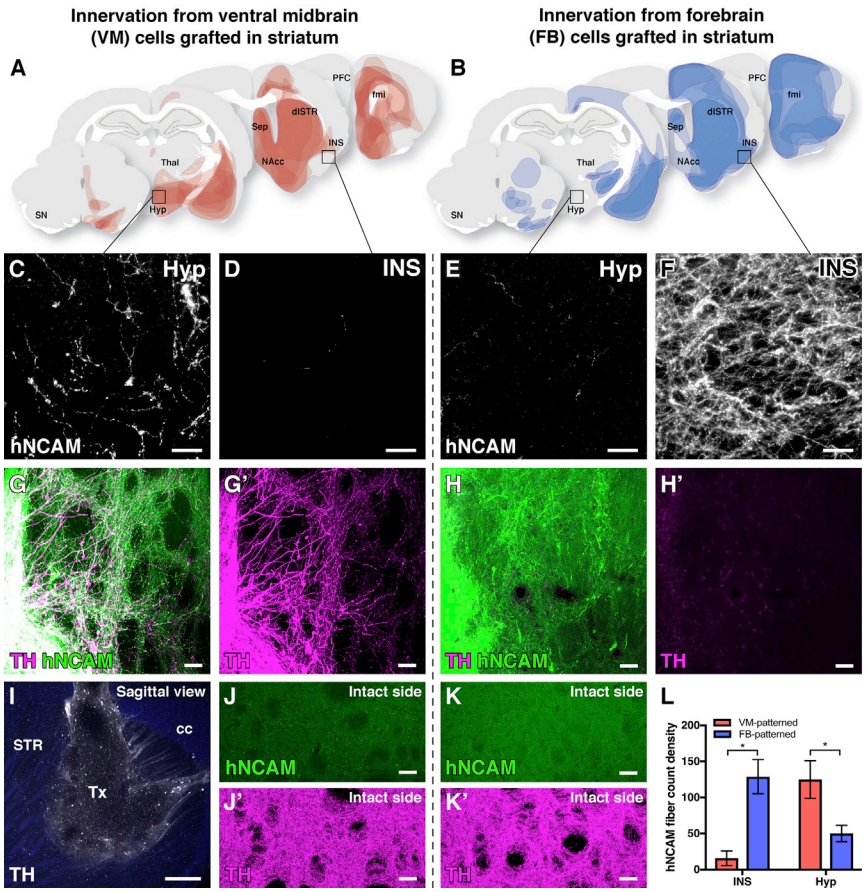

Figure 3. Comparison of Fiber Outgrowth from VM- versus FB-Patterned Grafts Placed into the Striatum

(A and B) Representations of graft-derived innervation of host structures as detected by hNCAM staining for grafts placed in the striatum of 6-OHDA lesioned rats after 24 weeks of graft maturation (cumulative data from n = 7 animals in A and n = 5 animals in B).

(C–F) VM-patterned neurons targeted fiber outgrowth toward the hypothalamus (Hyp) (C) but not INS (D), while FB-patterned neurons extensively INS (F) but not Hyp (E).

(G and H) Human (hNCAM$^+$) TH$^+$ fibers reinnervated the dopamine-depleted striatum from VM-patterned grafts (G), but not from FB-patterned grafts (H), after 24 weeks of maturation.

(I) Tissue clearing and light sheet microscopy provide an overview of VM graft-derived TH$^+$ fibers reinnervating the DA-depleted host striatum after 16 weeks of maturation, with endogenous autofluorescence shown in blue (see associated Video S3).

(J and K) Images of the contralateral (intact) side of the striatum in animals with (J) VM- and (K) FB-patterned grafts confirm the specificity of hNCAM labeling.

(L) Quantification of VM- versus FB-patterned hNCAM$^+$ innervation of host structures. (VM cells, n = 7 animals; FB cells, n = 5 animals; mean ± SEM, $p < 0.05$, $\alpha = 0.05$, two-way ANOVA with Bonferroni-corrected post hoc testing).

Scale bars represent 20 μm (C–F), 50 μm (G, H, J, and K), and 500 μm (I, sagittal plane). The TH channel in (G) and (H) are displayed with a higher exposure time than (J) and (K) to prevent over- and undersaturation. 6-OHDA, 6-hydroxydopamine; cc, corpus callosum; dlSTR, dorsolateral striatum; fmi, forceps minor; FB, forebrain; hNCAM, human neural cell adhesion molecule; Hyp, hypothalamus; INS, insular cortex; MFB, medial forebrain bundle; NAcc, nucleus accumbens; PFC, prefrontal cortex; Sep, septum; SN, substantia nigra; STR, striatum; TH, tyrosine hydroxylase; Thal, thalamus; Tx, transplant; VM, ventral midbrain.

striatum, subthalamic nucleus (STN), and substantia nigra pars reticulata and compacta (SNr/c) (Saunders et al., 2016); and FOXP2$^+$ arkypallidal neurons (Figure 5G), which project solely to the striatum (Abdi et al., 2015; Glajch et al., 2016) and may, therefore, represent an "ectopic" input to midbrain-patterned cells. In contrast, intranigral VM grafts also received inputs from PV$^+$ prototypic pallidal neurons (Figure 5E), but no inputs from FOXP2$^+$ arkypallidal neurons were observed, which is in agreement with the established anatomy of the arkypallidal projection. A summary of these results is illustrated schematically in Figure 5H.

The overlapping location and phenotypic identity of the ΔG-rabies-traced neurons in the cortex, striatum, and GPe suggested the possibility that host neurons synaptically contacting graft neurons could simultaneously innervate the SNc/r by collateral branches. In order to investigate this possibility, we injected cholera toxin B subunit (CTB; a conventional retrograde tracer) into the host substantia nigra immediately before the injection of the ΔG-rabies into intrastriatal VM-patterned grafts (Figures 6A and 6B). Indeed, we were able to detect mCherry and CTB double-labeled neurons in the PFC (Figure 6C), dlSTR (Figure 6D), and GPe (Figure 6E), indicating that the synaptic input to intrastriatal grafts is derived, at least in part, from the same cortical, striatal, and pallidal neurons that also innervate the host substantia nigra. As illustrated in Figure 6A, we propose that this dual output to intrastriatal grafts and the host nigra is established from collateral branches of presynaptic host neurons, either previously existing or newly formed within the striatum upon the introduction of graft neurons.

DA Denervation Alters Monosynaptic Inputs to the Transplant

To investigate if the presence of spared endogenous dopaminergic innervation in the striatum plays a role in host-to-graft synaptic integration, hESC-derived VM-patterned cells were transplanted into immunosuppressed intact or 6-OHDA-lesioned rats that were then sacrificed after 6 weeks of graft maturation and 1 week of graft-initiated monosynaptic rabies tracing. Histological analysis revealed that grafted neurons survived equally well under both conditions and generated grafts of comparable size (Figures 7A and 7B). An analysis of the origin of monosynaptic host inputs to graft neurons revealed no significant difference in the total amount of mCherry-labeled host neurons in intact and DA-depleted animals (Figure 7F). However, an

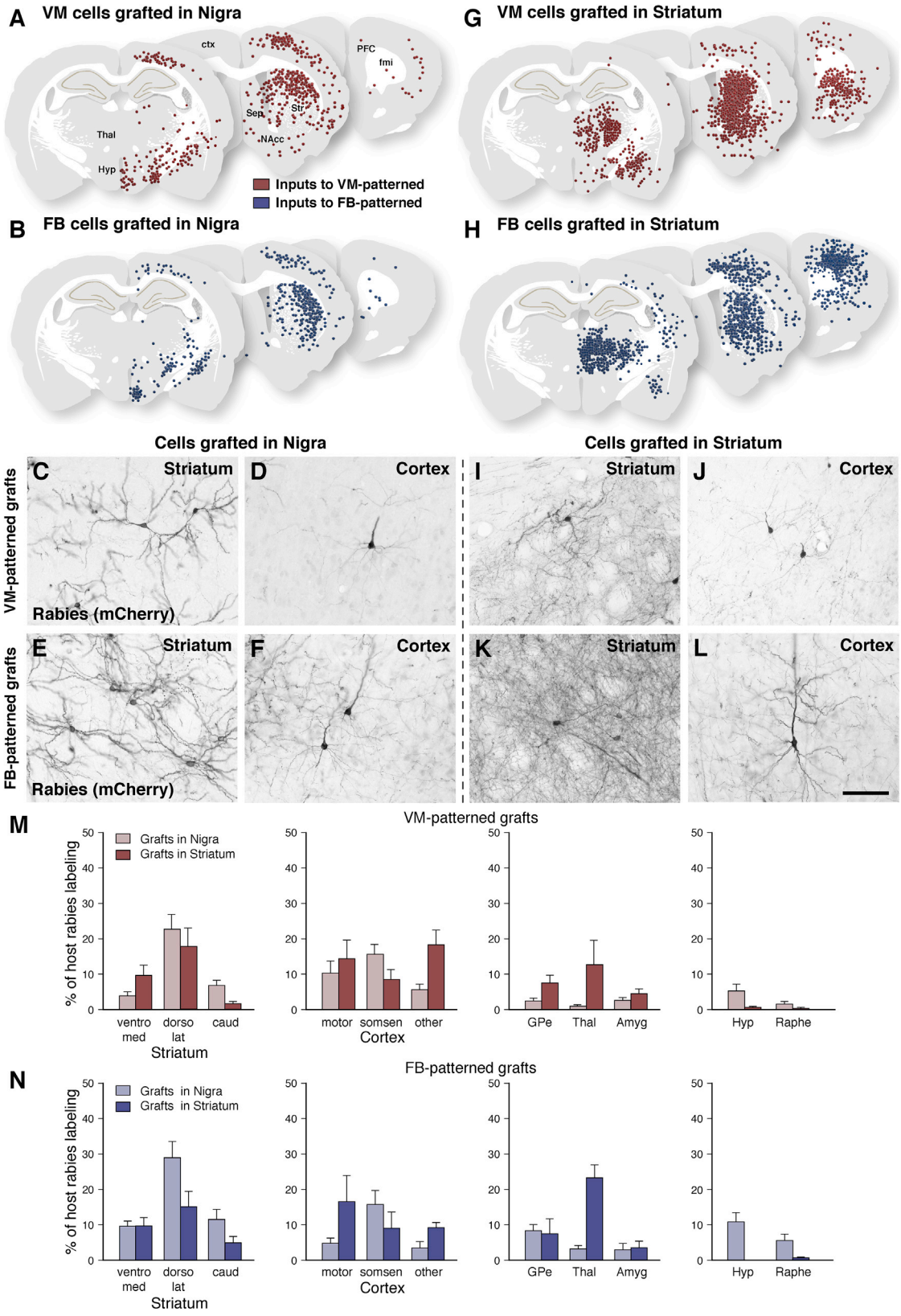

(legend on next page)

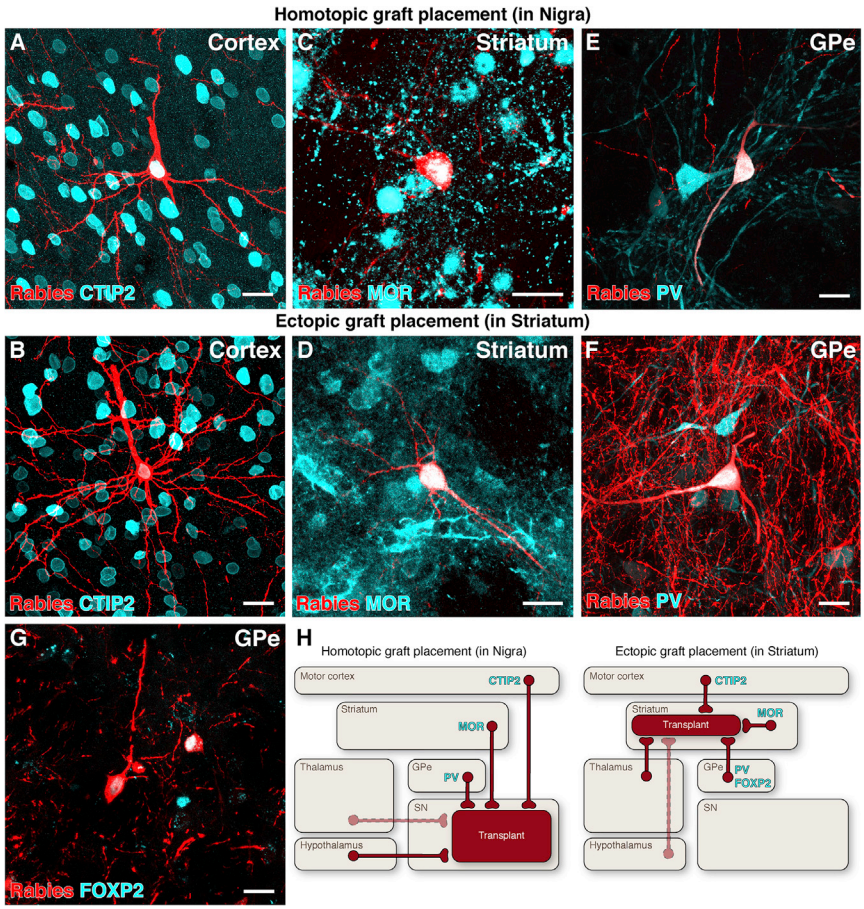

Figure 5. Phenotypic Similarity of Monosynaptic Inputs to Ectopic versus Homotopic VM-Patterned Grafts

(A–F) CTIP2$^+$ pyramidal neurons in motor cortex (A and B), MOR$^+$ medium spiny neurons in striatum (C and D), and PV$^+$ neurons in GPe (E, F) connected to both homotopic (intranigral) and ectopic (intrastriatal) grafts of VM-patterned neurons.

(G) FOXP2$^+$ GPe neurons were observed connecting only to grafts placed ectopically in the striatum.

(H) Schematic representations of the origin of host synaptic inputs to grafts placed in the substantia nigra versus the striatum. Solid lines represent host brain structures with extensive synaptic input to transplanted neurons, while dashed lines represent structures with comparatively scarce inputs.

Scale bars represent 20 μm. CTIP2, COUP-TF-interacting protein 2; FOXP2, forkhead box P2; GPe, external globus pallidus; MOR, mu-opioid receptor; PV, parvalbumin; SN, substantia nigra.

DISCUSSION

The use of fetal tissue as a cell replacement therapy to treat neurodegenerative disease has been explored clinically (Bachoud-Lévi, 2017; Barker et al., 2013; Kalladka et al., 2016). Although these studies have provided important proof-of-concept evidence for the viability of clinical cell replacement (Barker et al., 2013; Li et al., 2016; Lindvall et al., 1990), they also highlight the difficulties of reliably obtaining and utilizing fetal cell sources. To meet the demand for standardizable and transplantable cells in unlimited quantities, pluripotent stem cells (PSCs) are actively being developed as a source of therapeutic neurons. For example, it is now possible to obtain authentic, functional midbrain DA neurons from human PSCs in large numbers (Chen et al., 2016; Doi et al., 2014; Kirkeby et al., 2012; Kriks et al., 2011; Nolbrant et al., 2017), and stem-cell-based therapies for PD are now entering clinical trials (Barker et al., 2017; Kyoto Trial, 2018). These stem-cell-derived DA neurons are expected to function

increased proportion of inputs from the GPe was detected in the DA-depleted condition (Figures 7C–7E). Furthermore, we found that PV$^+$ pallidal neurons providing monosynaptic input to grafts were underrepresented compared to the observed proportion of PV$^+$ neurons in the total GPe (Figures 7G–7J) and that this bias was further enhanced by DA depletion of the host (Figures 7K and 7L). Taken together, these results demonstrate that host DA depletion is not a prerequisite for extensive host-graft connectivity but may shift the overall balance of synaptic input to graft neurons.

Figure 4. Role of Graft Phenotype and Placement on Synaptic Integration

(A–L) Schematic overviews (A, B, G, and H) of (C)–(F) and (I)–(L) 3,3′-diaminobenzidine (DAB)-developed staining of host synaptic inputs to VM- and FB-patterned grafts placed in either the nigra (A–F) or striatum (G–L). Each dot represents a ΔG-rabies$^+$ traced neuron tagged with mCherry collected from 1:8 series spanning 2.0, 1.4, or 2.4 mm (rostral to caudal) centered at each depicted section, cumulative from all animals in each group. Synaptic inputs to VM- and FB-patterned neurons originated from the same host structures when placed in the same location (compare A to B and G to H). On the other hand, synaptic inputs varied depending on the placement of the transplant (compare A to G and B to H). (A) Inputs to VM-patterned grafts placed in the nigra included host (C) striatal and (D) cortical neurons. (B) Inputs to FB-patterned grafts placed in the nigra included host (E) striatal and (F) cortical neurons. (G) Inputs to VM-patterned grafts placed in the striatum included host (I) striatal and (J) cortical neurons. (H) Inputs to FB-patterned grafts placed in the striatum included host (K) striatal and (L) cortical neurons.

(M and N) Quantification of the percentage of rabies$^+$ neurons per anatomical structure over the total number of ΔG-rabies$^+$ neurons per brain in animals grafted with (M) VM- or (N) FB-patterned cells (VM cells in SN, n = 5 animals; FB cells in SN, n = 6 animals; VM cells in striatum, n = 7 animals; FB cells in striatum, n = 5 animals). Data presented as mean + SEM. See also Figure S2.

Scale bar represents 20 μm (C–F and I–L). Amyg, amygdala; caud, caudal striatum; ctx, cortex; dorso lat, dorsolateral striatum; FB, forebrain; fmi, forceps minor; GPe, external globus pallidus; Hyp, hypothalamus; motor, motor cortex; NAcc, nucleus accumbens; PFC, prefrontal cortex; sep, septum; somsen, somatosensory cortex; Str, striatum; Thal, thalamus; VM, ventral midbrain; ventro med, ventromedial striatum.

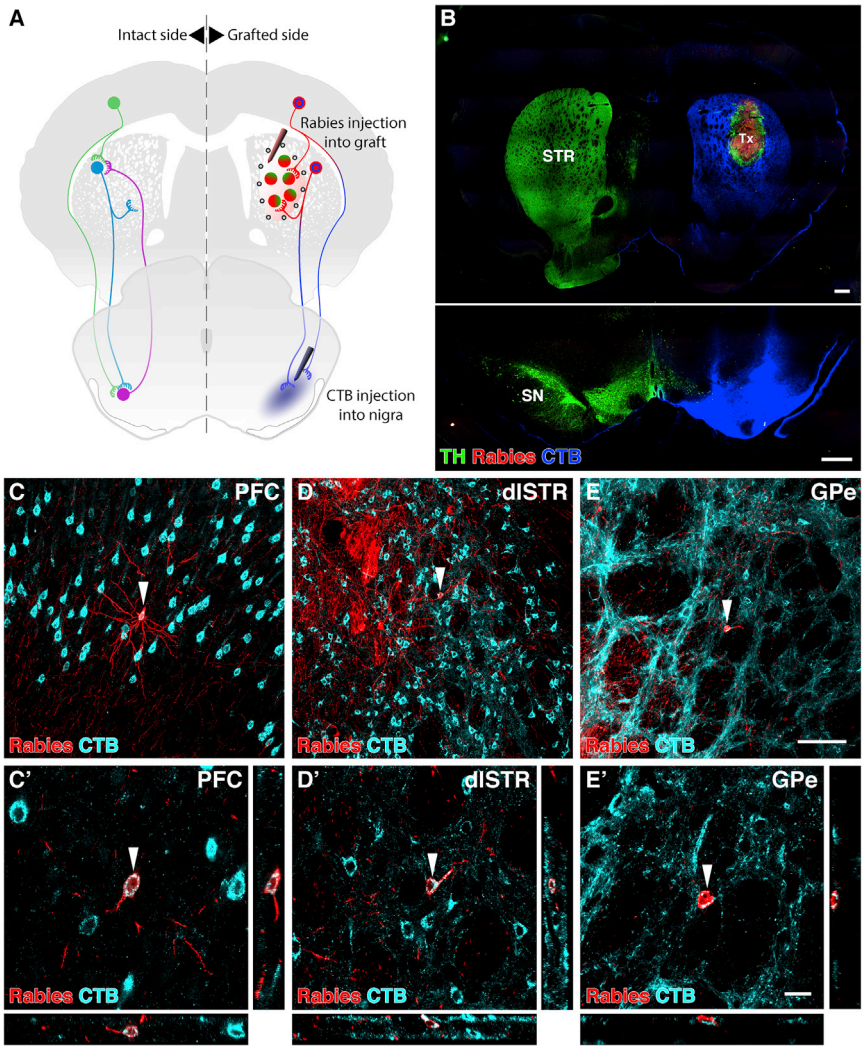

Figure 6. Host Neurons Providing Monosynaptic Input to VM-Patterned Grafts Placed in the Striatum Simultaneously Collateralize on Neurons in the Substantia Nigra

(A) Schematic of monosynaptic EnvA ΔG-rabies tracing initiated from striatal grafts, with simultaneous conventional retrograde cholera toxin subunit B (CTB) tracing of projections to the substantia nigra.

(B) Sections through striatum depicting the graft and rabies injection site, and the substantia nigra depicting the lesion and CTB injection site.

(C–E) Host prefrontal cortical (C), medium spiny striatal (D), and pallidal neurons (E) were labeled with both CTB and rabies. Arrowheads indicate neurons imaged with confocal microscopy in (C'), (D'), and (E'). These neurons simultaneously synapse with graft neurons and maintain a collateral projection to the substantia nigra.

Scale bars represent 500 μm (B), 100 μm (C, D, and E), and 20 μm (C', D', and E'). Images in (B) is digitally stitched from multiple high-magnification images. CTB, cholera toxin subunit B; dlSTR, dorsolateral striatum; GPe, external globus pallidus; PFC, prefrontal cortex; SN, substantia nigra; STR, striatum; TH, tyrosine hydroxylase; Tx, transplant.

en par with human fetal cells but in a more reliable manner because the production of therapeutic stem cell products can be performed using standardized methods and strict quality control that are not possible to achieve with the collection and use of fetal human tissue.

This study was designed to gain a better understanding of which factors control graft-derived innervation and synaptic integration of hESC-derived grafts into host neural circuitry after transplantation. First, two types of hESC-derived progenitors (VM- and FB-patterned) were transplanted into the midbrain or striatum of 6-OHDA-lesioned adult rats, and graft-derived axonal outgrowth and innervation of the host brain was assessed and compared after 6 months. This revealed that although VM-patterned cells grafted to the nigra were able to recapitulate the endogenous mesencephalic dopaminergic pathway and innervate appropriate A9 (dlSTR) and A10 (NAcc and PFC) FB target structures, FB-patterned neurons did not elicit innervation toward the dlSTR and instead preferentially innervated host cortical and limbic structures. These results point to cell-intrinsic factors determining the fiber outgrowth patterns of transplanted hESC-derived neurons and reinforce the importance of the correct patterning of grafted neurons to achieve sufficient innervation of appropriate host target structures (Espuny-Camacho et al., 2018; Gaillard et al., 2009; Hargus et al., 2010; Isacson and Deacon, 1996; Michelsen et al., 2015; Terrigno et al., 2018).

Second, we used monosynaptic tracing to dissect the effect of graft placement and cell phenotype on long-term host-to-graft monosynaptic connectivity. The widespread host-to-graft inputs that we previously observed 6 weeks after grafting (Cardoso et al., 2018) were maintained after 24 weeks of graft maturation. Sustained synaptic integration between host and graft is a promising observation in a clinical context, where patients will ideally benefit from graft function for decades. This experiment also revealed that the phenotype of the grafted cells had no detectable effect on global synaptic integration, as the anatomical origin and extent of host synaptic inputs to VM- and FB-patterned neurons were similar when grafted to the same location.

Next, we investigated whether graft placement would have an effect on host-graft synaptic integration. In clinical applications for the treatment of PD, fetal VM grafts are directly placed into the caudate and putamen (Barker et al., 2013). This strategy places the tissue in close proximity to the targets of nigral dopaminergic innervation, thereby expediting and ensuring sufficient dopaminergic innervation of the host putamen in order to elicit therapeutic benefit in PD patients. Similarly, in experimental models of PD, intrastriatal grafts of VM tissue more efficiently

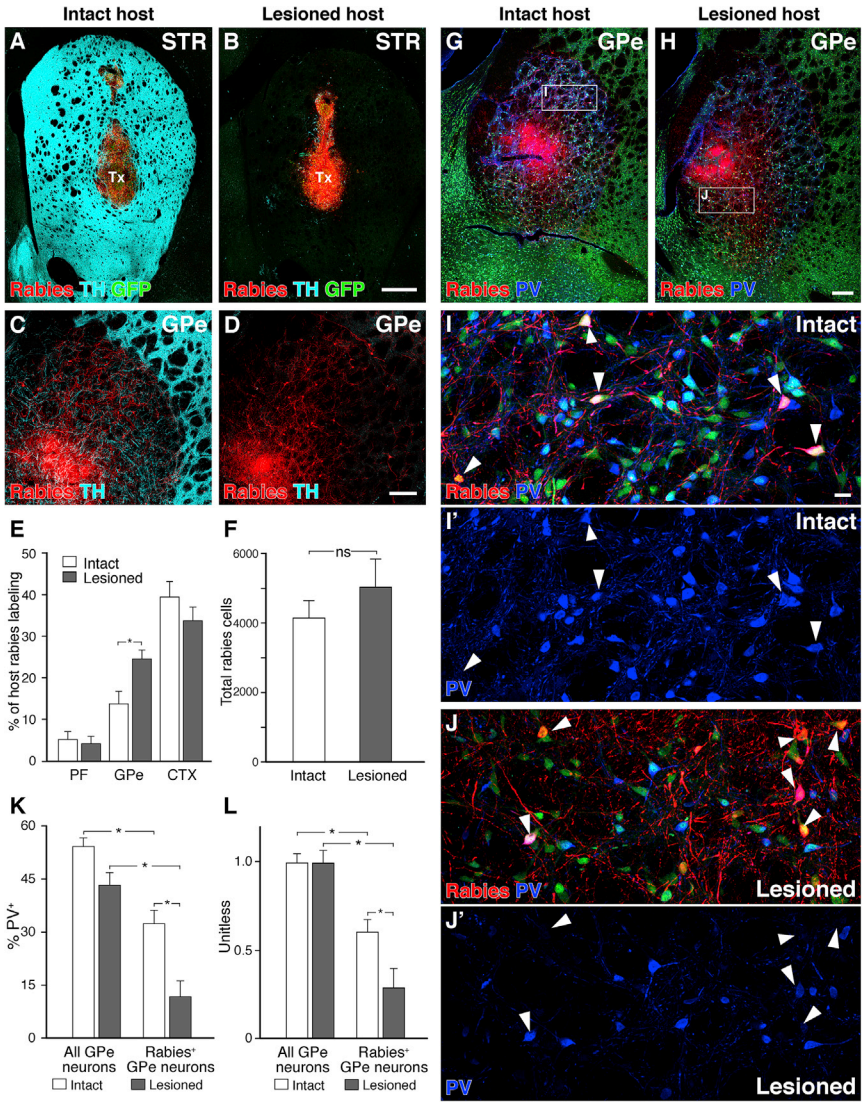

Figure 7. Monosynaptic Inputs to VM-Patterned Grafts in Intact versus 6-OHDA Lesioned Rats

(A and B) VM-patterned cells placed in the striatum of intact (A) or 6-OHDA-lesioned rats (B) generate grafts of comparable size.

(C–E) Lesioned host animals had an increased number of rabies-labeled neurons in the GPe (C and D), as well as an increased fraction of GPe inputs normalized to labeling in the entire brain (E).

(F) The overall number of ΔG-rabies-labeled host neurons was not significantly different between intact and lesioned hosts.

(G–J) ΔG-rabies-labeled GPe neurons were PV^+ less frequently than the observed PV^+ proportion of all GPe neurons in both intact (G, detail in I) and lesioned (H, detail in J) hosts.

(K and L) This bias was increased with lesion, both before (K) and after (L) normalization for a reduced total PV^+ neuron frequency observed in the GPe in lesioned hosts. (Intact, n = 5 animals; lesioned, n = 5 animals; mean + SEM, $p < 0.05$, $\alpha = 0.05$; (E, K, and L) Two-way ANOVA with Bonferroni-corrected post hoc testing; F unpaired two-tailed t test, $p = 0.36$.) Scale bars represent 500 μm (A and B), 200 μm (C, D, G, and H), and 20 μm (I and J). Images in (A)–(D), (G), and (H) are digitally stitched from multiple high-magnification images. CTX, cortex; GFP, green fluorescent protein; GPe, external globus pallidus; NeuN, neuronal nuclei; PF, parafascicular nucleus; PV, parvalbumin; STR, striatum; TH, tyrosine hydroxylase; Tx, transplant.

restore motor function than intranigral grafts (Winkler et al., 2000), and intrastriatal graft placement is most commonly used for the preclinical assessment of stem-cell-derived DA neurons (Kikuchi et al., 2017; Kirkeby et al., 2012; Kriks et al., 2011). Despite this ectopic placement of midbrain-patterned cells in the FB, these grafts have been shown to provide robust long-term effects in patients and animal models, suggesting an appropriate regulation of DA release after intrastriatal transplantation (Barker et al., 2013; Kefalopoulou et al., 2014).

Here, we show that dopaminergic grafts transplanted both homotopically to the midbrain and ectopically to the striatum receive inputs from cortex, striatum, and globus pallidus. Neurons in these locations are known to regulate SNc DA neuron function and to send collateral projections within the striatum (Molyneaux et al., 2007; Shepherd, 2013; Smith et al., 2016; Watabe-Uchida et al., 2012). This arrangement provides an anatomical substrate whereby intrastriatal grafts, despite their ectopic location, can nevertheless receive input from functionally appropriate subtypes of host excitatory (cortical) and inhibitory (striatal and pallidal) neurons. As illustrated schematically in Figure 5H, this host-to-graft connectivity may provide important regulatory control of the grafted neurons and help to explain the appropriately regulated DA release from, and clinical efficacy of, "ectopic" intrastriatal VM-patterned grafts. Using two types of tracers, we provide evidence that host neurons have the capacity to simultaneously innervate the grafted cells in the striatum and the endogenous neurons in the substantia nigra.

Third, we found that VM-patterned neurons were able to integrate into host circuitry to a similar extent when grafted into the intact or DA-denervated striatum, representing two extremes of the clinical progression of DA loss in PD patients. This result has promising implications for clinical translation, considering that DA neuron grafts will be placed in the putamen of PD patients with varying degrees of dopaminergic denervation (Barker et al., 2017; Kordower et al., 2013). Interestingly, we also observed an increase in pallidal inputs upon DA depletion of the host. This increase in total GPe inputs was accompanied by a decrease in the proportion of PV^+ GPe inputs, suggesting a shifted balance of input from the two major classes of GPe neurons—the STN/substantia nigra (SN)-projecting prototypical and the striatum-projecting arkypallidal neurons—in response to DA denervation.

Arkypallidal neurons have been shown to respond to striatal DA denervation (Hernández et al., 2015) and to play a role in the modulation of motor behavior in DA-depleted mice (Mastro et al., 2017) and may, thus, be of particular interest as potential regulators of intrastriatal graft function. In general, the valence and functional impact of each individual type of host-graft input is likely to depend on both direct (monosynaptic) contacts with graft DA neurons, as well as on di- or poly-synaptic relays to graft DA neurons by other (non-dopaminergic) graft neuronal subtypes.

In summary, we show that cell-intrinsic factors are involved in determining the pattern and extent of hESC graft-derived innervation, while presynaptic integration is impacted to a greater extent by the location of the graft in the host brain. We also demonstrate that VM-patterned grafts placed ectopically in the striatum receive synaptic inputs from major excitatory (cortical) and inhibitory (striatal and pallidal) populations known to innervate the substantia nigra and that the balance of inputs from subpopulations of pallidal neurons shifts upon DA-depletion of the host. The functional implications of altered input balance to VM-patterned grafts as a consequence of DA depletion should be further investigated, in the context of the design of dopaminergic cell replacement therapy clinical trials. Our findings also have implications for the design of future cell therapeutic strategies for the treatment of other neurodegenerative diseases, by highlighting the importance of properly patterned PSC products for targeted graft-derived axonal innervation and by providing an understanding of how innervation and integration into circuits after transplantation is regulated at the cellular level, which will be important for devising future strategies aimed at more complete neural circuit repair.

STAR★METHODS

Detailed methods are provided in the online version of this paper and include the following:

- KEY RESOURCES TABLE
- LEAD CONTACT AND MATERIALS AVAILABILITY
- EXPERIMENTAL MODEL AND SUBJECT DETAILS
  - hESC differentiation and transgene expression
  - Research animals
- METHOD DETAILS
  - Study design
  - ΔG-rabies production
  - Surgical procedures
  - Tissue clearing
  - Light sheet microscopy
  - Immunohistochemistry
  - Immunocytochemistry
  - qRT-PCR
  - Microscopy and image analysis
- QUANTIFICATION AND STATISTICAL ANALYSIS
- DATA AND CODE AVAILABILITY

SUPPLEMENTAL INFORMATION

Supplemental Information can be found online at https://doi.org/10.1016/j.celrep.2019.08.058.

ACKNOWLEDGMENTS

The authors thank Michael Sparrenius, Susanne Geres, Sol da Rocha Baez, Jenny Johansson, and Marie Persson Vejgården for excellent technical assistance. The research leading to these results has received funding from the New York Stem Cell Foundation; the European Research Council under the European Union's Seventh Framework Programme: FP/2007-2013 NeuroStemcellRepair (no. 602278); ERC Grant Agreement no. 30971; the Swedish Research Council (grant agreement 2016-00873); 2018-02608; Swedish Parkinson Foundation (Parkinsonfonden); Swedish Brain Foundation; the Strategic Research Area at Lund University Multipark (Multidisciplinary research in PD); and Knut and Alice Wallenberg Stiftelse (KAW 2018-0040). M.P. is a New York Stem Cell Foundation Robertson Investigator.

AUTHOR CONTRIBUTIONS

A.F.A. and T.C. conceived the project, designed and performed experiments, analyzed results in the project, and wrote part of the paper; S.N. and J.N.W. performed cell differentiations and partook in planning and analysis of experiments; D.B.H. performed and interpreted *in vivo* experiments; B.M. performed 3D mapping, microscopic analysis including LSM, and assembled the figures; U.J. developed and performed the clearing method; S.G. designed and interpreted experiments; A.B. and M.P. conceived the project, designed experiments, interpreted results and wrote the paper with input from all authors.

DECLARATION OF INTERESTS

M.P. is the owner of Parmar Cells AB and co-inventor of the U.S. patent application 15/093,927 owned by Biolamina AB and EP17181588 owned by Miltenyi Biotech.

Received: February 11, 2019
Revised: April 30, 2019
Accepted: August 19, 2019
Published: September 24, 2019

REFERENCES

Abdi, A., Mallet, N., Mohamed, F.Y., Sharott, A., Dodson, P.D., Nakamura, K.C., Suri, S., Avery, S.V., Larvin, J.T., Garas, F.N., et al. (2015). Prototypic and arkypallidal neurons in the dopamine-intact external globus pallidus. J. Neurosci. *35*, 6667–6688.

Adams, J.C. (1992). Biotin amplification of biotin and horseradish peroxidase signals in histochemical stains. J. Histochem. Cytochem. *40*, 1457–1463.

Aldrin-Kirk, P., Heuer, A., Wang, G., Mattsson, B., Lundblad, M., Parmar, M., and Björklund, T. (2016). DREADD Modulation of Transplanted DA Neurons Reveals a Novel Parkinsonian Dyskinesia Mechanism Mediated by the Serotonin 5-HT6 Receptor. Neuron *90*, 955–968.

Bachoud-Lévi, A.C. (2017). From open to large-scale randomized cell transplantation trials in Huntington's disease: Lessons from the multicentric intracerebral grafting in Huntington's disease trial (MIG-HD) and previous pilot studies. Prog. Brain Res. *230*, 227–261.

Barker, R.A., Barrett, J., Mason, S.L., and Björklund, A. (2013). Fetal dopaminergic transplantation trials and the future of neural grafting in Parkinson's disease. Lancet Neurol. *12*, 84–91.

Barker, R.A., Parmar, M., Studer, L., and Takahashi, J. (2017). Human Trials of Stem Cell-Derived Dopamine Neurons for Parkinson's Disease: Dawn of a New Era. Cell Stem Cell *21*, 569–573.

Cardoso, T., Adler, A.F., Mattsson, B., Hoban, D.B., Nolbrant, S., Wahlestedt, J.N., Kirkeby, A., Grealish, S., Björklund, A., and Parmar, M. (2018). Target-specific forebrain projections and appropriate synaptic inputs of hESC-derived dopamine neurons grafted to the midbrain of parkinsonian rats. J. Comp. Neurol. *526*, 2133–2146.

Chen, Y., Xiong, M., Dong, Y., Haberman, A., Cao, J., Liu, H., Zhou, W., and Zhang, S.C. (2016). Chemical Control of Grafted Human PSC-Derived Neurons in a Mouse Model of Parkinson's Disease. Cell Stem Cell *18*, 817–826.

Doerr, J., Schwarz, M.K., Wiedermann, D., Leinhaas, A., Jakobs, A., Schloen, F., Schwarz, I., Diedenhofen, M., Braun, N.C., Koch, P., et al. (2017). Whole-brain 3D mapping of human neural transplant innervation. Nat. Commun. *8*, 14162.

Doi, D., Samata, B., Katsukawa, M., Kikuchi, T., Morizane, A., Ono, Y., Sekiguchi, K., Nakagawa, M., Parmar, M., and Takahashi, J. (2014). Isolation of human induced pluripotent stem cell-derived dopaminergic progenitors by cell sorting for successful transplantation. Stem Cell Reports *2*, 337–350.

Espuny-Camacho, I., Michelsen, K.A., Linaro, D., Bilheu, A., Acosta-Verdugo, S., Herpoel, A., Giugliano, M., Gaillard, A., and Vanderhaeghen, P. (2018). Human Pluripotent Stem-Cell-Derived Cortical Neurons Integrate Functionally into the Lesioned Adult Murine Visual Cortex in an Area-Specific Way. Cell Rep. *23*, 2732–2743.

Fisher, L.J., Young, S.J., Tepper, J.M., Groves, P.M., and Gage, F.H. (1991). Electrophysiological characteristics of cells within mesencephalon suspension grafts. Neuroscience *40*, 109–122.

Gaillard, A., Decressac, M., Frappé, I., Fernagut, P.O., Prestoz, L., Besnard, S., and Jaber, M. (2009). Anatomical and functional reconstruction of the nigrostriatal pathway by intranigral transplants. Neurobiol. Dis. *35*, 477–488.

Gerfen, C.R. (1992). The neostriatal mosaic: multiple levels of compartmental organization. Trends Neurosci. *15*, 133–139.

Glajch, K.E., Kelver, D.A., Hegeman, D.J., Cui, Q., Xenias, H.S., Augustine, E.C., Hernández, V.M., Verma, N., Huang, T.Y., Luo, M., et al. (2016). Npas1+ Pallidal Neurons Target Striatal Projection Neurons. J. Neurosci. *36*, 5472–5488.

Grealish, S., Jönsson, M.E., Li, M., Kirik, D., Björklund, A., and Thompson, L.H. (2010). The A9 dopamine neuron component in grafts of ventral mesencephalon is an important determinant for recovery of motor function in a rat model of Parkinson's disease. Brain *133*, 482–495.

Grealish, S., Diguet, E., Kirkeby, A., Mattsson, B., Heuer, A., Bramoulle, Y., Van Camp, N., Perrier, A.L., Hantraye, P., Björklund, A., and Parmar, M. (2014). Human ESC-derived dopamine neurons show similar preclinical efficacy and potency to fetal neurons when grafted in a rat model of Parkinson's disease. Cell Stem Cell *15*, 653–665.

Grealish, S., Heuer, A., Cardoso, T., Kirkeby, A., Jönsson, M., Johansson, J., Björklund, A., Jakobsson, J., and Parmar, M. (2015). Monosynaptic Tracing using Modified Rabies Virus Reveals Early and Extensive Circuit Integration of Human Embryonic Stem Cell-Derived Neurons. Stem Cell Reports *4*, 975–983.

Hargus, G., Cooper, O., Deleidi, M., Levy, A., Lee, K., Marlow, E., Yow, A., Soldner, F., Hockemeyer, D., Hallett, P.J., et al. (2010). Differentiated Parkinson patient-derived induced pluripotent stem cells grow in the adult rodent brain and reduce motor asymmetry in Parkinsonian rats. Proc. Natl. Acad. Sci. USA *107*, 15921–15926.

Hernández, V.M., Hegeman, D.J., Cui, Q., Kelver, D.A., Fiske, M.P., Glajch, K.E., Pitt, J.E., Huang, T.Y., Justice, N.J., and Chan, C.S. (2015). Parvalbumin+ Neurons and Npas1+ Neurons Are Distinct Neuron Classes in the Mouse External Globus Pallidus. J. Neurosci. *35*, 11830–11847.

Isacson, O., and Deacon, T.W. (1996). Specific axon guidance factors persist in the adult brain as demonstrated by pig neuroblasts transplanted to the rat. Neuroscience *75*, 827–837.

Isacson, O., Deacon, T.W., Pakzaban, P., Galpern, W.R., Dinsmore, J., and Burns, L.H. (1995). Transplanted xenogeneic neural cells in neurodegenerative disease models exhibit remarkable axonal target specificity and distinct growth patterns of glial and axonal fibres. Nat. Med. *1*, 1189–1194.

Kalladka, D., Sinden, J., Pollock, K., Haig, C., McLean, J., Smith, W., McConnachie, A., Santosh, C., Bath, P.M., Dunn, L., and Muir, K.W. (2016). Human neural stem cells in patients with chronic ischaemic stroke (PISCES): a phase 1, first-in-man study. Lancet *388*, 787–796.

Kefalopoulou, Z., Politis, M., Piccini, P., Mencacci, N., Bhatia, K., Jahanshahi, M., Widner, H., Rehncrona, S., Brundin, P., Björklund, A., et al. (2014). Long-term clinical outcome of fetal cell transplantation for Parkinson disease: two case reports. JAMA Neurol. *71*, 83–87.

Kikuchi, T., Morizane, A., Doi, D., Magotani, H., Onoe, H., Hayashi, T., Mizuma, H., Takara, S., Takahashi, R., Inoue, H., et al. (2017). Human iPS cell-derived dopaminergic neurons function in a primate Parkinson's disease model. Nature *548*, 592–596.

Kirkeby, A., Grealish, S., Wolf, D.A., Nelander, J., Wood, J., Lundblad, M., Lindvall, O., and Parmar, M. (2012). Generation of regionally specified neural progenitors and functional neurons from human embryonic stem cells under defined conditions. Cell Rep. *1*, 703–714.

Kirkeby, A., Nolbrant, S., Tiklova, K., Heuer, A., Kee, N., Cardoso, T., Ottosson, D.R., Lelos, M.J., Rifes, P., Dunnett, S.B., et al. (2017). Predictive Markers Guide Differentiation to Improve Graft Outcome in Clinical Translation of hESC-Based Therapy for Parkinson's Disease. Cell Stem Cell *20*, 135–148.

Kordower, J.H., Olanow, C.W., Dodiya, H.B., Chu, Y., Beach, T.G., Adler, C.H., Halliday, G.M., and Bartus, R.T. (2013). Disease duration and the integrity of the nigrostriatal system in Parkinson's disease. Brain *136*, 2419–2431.

Kriks, S., Shim, J.W., Piao, J., Ganat, Y.M., Wakeman, D.R., Xie, Z., Carrillo-Reid, L., Auyeung, G., Antonacci, C., Buch, A., et al. (2011). Dopamine neurons derived from human ES cells efficiently engraft in animal models of Parkinson's disease. Nature *480*, 547–551.

Kyoto Trial (2018). Announcement of physician-initiated clinical trials for Parkinson's disease. http://www.cira.kyoto-u.ac.jp/e/pressrelease/news/180730-170000.html.

Li, W., Englund, E., Widner, H., Mattsson, B., van Westen, D., Lätt, J., Rehncrona, S., Brundin, P., Björklund, A., Lindvall, O., and Li, J.Y. (2016). Extensive graft-derived dopaminergic innervation is maintained 24 years after transplantation in the degenerating parkinsonian brain. Proc. Natl. Acad. Sci. USA *113*, 6544–6549.

Lindvall, O., and Kokaia, Z. (2011). Stem cell research in stroke: how far from the clinic? Stroke *42*, 2369–2375.

Lindvall, O., Brundin, P., Widner, H., Rehncrona, S., Gustavii, B., Frackowiak, R., Leenders, K.L., Sawle, G., Rothwell, J.C., Marsden, C.D., et al. (1990). Grafts of fetal dopamine neurons survive and improve motor function in Parkinson's disease. Science *247*, 574–577.

Mastro, K.J., Zitelli, K.T., Willard, A.M., Leblanc, K.H., Kravitz, A.V., and Gittis, A.H. (2017). Cell-specific pallidal intervention induces long-lasting motor recovery in dopamine-depleted mice. Nat. Neurosci. *20*, 815–823.

Michelsen, K.A., Acosta-Verdugo, S., Benoit-Marand, M., Espuny-Camacho, I., Gaspard, N., Saha, B., Gaillard, A., and Vanderhaeghen, P. (2015). Area-specific reestablishment of damaged circuits in the adult cerebral cortex by cortical neurons derived from mouse embryonic stem cells. Neuron *85*, 982–997.

Molyneaux, B.J., Arlotta, P., Menezes, J.R., and Macklis, J.D. (2007). Neuronal subtype specification in the cerebral cortex. Nat. Rev. Neurosci. *8*, 427–437.

Niclis, J.C., Gantner, C.W., Hunt, C.P.J., Kauhausen, J.A., Durnall, J.C., Haynes, J.M., Pouton, C.W., Parish, C.L., and Thompson, L.H. (2017). A PITX3-EGFP Reporter Line Reveals Connectivity of Dopamine and Non-dopamine Neuronal Subtypes in Grafts Generated from Human Embryonic Stem Cells. Stem Cell Reports *9*, 868–882.

Nolbrant, S., Heuer, A., Parmar, M., and Kirkeby, A. (2017). Generation of high-purity human ventral midbrain dopaminergic progenitors for in vitro maturation and intracerebral transplantation. Nat. Protoc. *12*, 1962–1979.

Paxinos, G., and Watson, C. (2005). The Rat Brain in Stereotaxic Coordinates, Fifth Edition (Academic Press).

Piccini, P., Brooks, D.J., Björklund, A., Gunn, R.N., Grasby, P.M., Rimoldi, O., Brundin, P., Hagell, P., Rehncrona, S., Widner, H., and Lindvall, O. (1999). Dopamine release from nigral transplants visualized in vivo in a Parkinson's patient. Nat. Neurosci. *2*, 1137–1140.

Renier, N., Wu, Z., Simon, D.J., Yang, J., Ariel, P., and Tessier-Lavigne, M. (2014). iDISCO: a simple, rapid method to immunolabel large tissue samples for volume imaging. Cell *159*, 896–910.

Saunders, A., Huang, K.W., and Sabatini, B.L. (2016). Globus Pallidus Externus Neurons Expressing parvalbumin Interconnect the Subthalamic Nucleus and Striatal Interneurons. PLoS One *11*, e0149798.

Schindelin, J., Arganda-Carreras, I., Frise, E., Kaynig, V., Longair, M., Pietzsch, T., Preibisch, S., Rueden, C., Saalfeld, S., Schmid, B., et al. (2012). Fiji: an open-source platform for biological-image analysis. Nat. Methods *9*, 676–682.

Shepherd, G.M. (2013). Corticostriatal connectivity and its role in disease. Nat. Rev. Neurosci. *14*, 278–291.

Shirai, H., Mandai, M., Matsushita, K., Kuwahara, A., Yonemura, S., Nakano, T., Assawachananont, J., Kimura, T., Saito, K., Terasaki, H., et al. (2016). Transplantation of human embryonic stem cell-derived retinal tissue in two primate models of retinal degeneration. Proc. Natl. Acad. Sci. USA *113*, E81–E90.

Smith, J.B., Klug, J.R., Ross, D.L., Howard, C.D., Hollon, N.G., Ko, V.I., Hoffman, H., Callaway, E.M., Gerfen, C.R., and Jin, X. (2016). Genetic-Based Dissection Unveils the Inputs and Outputs of Striatal Patch and Matrix Compartments. Neuron *91*, 1069–1084.

Sørensen, A.T., Thompson, L., Kirik, D., Björklund, A., Lindvall, O., and Kokaia, M. (2005). Functional properties and synaptic integration of genetically labelled dopaminergic neurons in intrastriatal grafts. Eur. J. Neurosci. *21*, 2793–2799.

Steger, C. (1998). An unbiased detector of curvilinear structures. IEEE Trans Pattern Anal Mach Intell *20*, 113–125.

Steinbeck, J.A., Choi, S.J., Mrejeru, A., Ganat, Y., Deisseroth, K., Sulzer, D., Mosharov, E.V., and Studer, L. (2015). Optogenetics enables functional analysis of human embryonic stem cell-derived grafts in a Parkinson's disease model. Nat. Biotechnol. *33*, 204–209.

Studer, L. (2017). Strategies for bringing stem cell-derived dopamine neurons to the clinic-The NYSTEM trial. Prog. Brain Res. *230*, 191–212.

Takahashi, J. (2017). Strategies for bringing stem cell-derived dopamine neurons to the clinic: The Kyoto trial. Prog. Brain Res. *230*, 213–226.

Terrigno, M., Busti, I., Alia, C., Pietrasanta, M., Arisi, I., D'Onofrio, M., Caleo, M., and Cremisi, F. (2018). Neurons Generated by Mouse ESCs with Hippocampal or Cortical Identity Display Distinct Projection Patterns When Co-transplanted in the Adult Brain. Stem Cell Reports *10*, 1016–1029.

Thompson, L., Barraud, P., Andersson, E., Kirik, D., and Björklund, A. (2005). Identification of dopaminergic neurons of nigral and ventral tegmental area subtypes in grafts of fetal ventral mesencephalon based on cell morphology, protein expression, and efferent projections. J. Neurosci. *25*, 6467–6477.

Thompson, L.H., Grealish, S., Kirik, D., and Björklund, A. (2009). Reconstruction of the nigrostriatal dopamine pathway in the adult mouse brain. Eur. J. Neurosci. *30*, 625–638.

Tornero, D., Tsupykov, O., Granmo, M., Rodriguez, C., Grønning-Hansen, M., Thelin, J., Smozhanik, E., Laterza, C., Wattananit, S., Ge, R., et al. (2017). Synaptic inputs from stroke-injured brain to grafted human stem cell-derived neurons activated by sensory stimuli. Brain *140*, 692–706.

Watabe-Uchida, M., Zhu, L., Ogawa, S.K., Vamanrao, A., and Uchida, N. (2012). Whole-brain mapping of direct inputs to midbrain dopamine neurons. Neuron *74*, 858–873.

Whiting, P., Kerby, J., Coffey, P., da Cruz, L., and McKernan, R. (2015). Progressing a human embryonic stem-cell-based regenerative medicine therapy towards the clinic. Philos. Trans. R. Soc. Lond. B Biol. Sci. *370*, 20140375.

Wickersham, I.R., Lyon, D.C., Barnard, R.J., Mori, T., Finke, S., Conzelmann, K.K., Young, J.A., and Callaway, E.M. (2007). Monosynaptic restriction of transsynaptic tracing from single, genetically targeted neurons. Neuron *53*, 639–647.

Wictorin, K., Brundin, P., Sauer, H., Lindvall, O., and Björklund, A. (1992). Long distance directed axonal growth from human dopaminergic mesencephalic neuroblasts implanted along the nigrostriatal pathway in 6-hydroxydopamine lesioned adult rats. J. Comp. Neurol. *323*, 475–494.

Winkler, C., Kirik, D., Björklund, A., and Dunnett, S.B. (2000). Transplantation in the rat model of Parkinson's disease: ectopic versus homotopic graft placement. Prog. Brain Res. *127*, 233–265.

STAR★METHODS

KEY RESOURCES TABLE

REAGENT or RESOURCE	SOURCE	IDENTIFIER
Antibodies		
Goat Anti-Cholera Toxin B Subunit	List Biological	Cat#703; RRID: AB_10013220
Rabbit Anti-CTIP2	Abcam	Cat#ab28448; RRID: AB_1140055
Rabbit Anti-DARPP-32	Cell Signaling Technology	Cat#2306; RRID: AB_823479
Goat Anti-FOXA2	Santa Cruz Biotechnology	Cat#sc-6554; RRID: AB_2262810
Mouse Anti-FOXP2	Millipore	Cat#MABE415; RRID: AB_2721039
Chicken Anti-GFP	Abcam	Cat#ab13970; RRID: AB_300798
Mouse Anti-hNCAM	Santa Cruz Biotechnology	Cat#sc-106; RRID: AB_627128
Mouse Anti-HuNu	Millipore	Cat#MAB1281; RRID: AB_94090
Rabbit Anti-LMX-1	Millipore	Cat#AB10533; RRID: AB_10805970
Goat Anti-mCherry	SICGEN	Cat#AB0040-200; RRID: AB_2333092
Rabbit Anti-mCherry	Abcam	Cat#ab167453; RRID: AB_2571870
Guinea Pig Anti-MOR	Millipore	Cat#AB5509; RRID: AB_177511
Rabbit Anti-NKX2.1 (TTF1)	Abcam	Cat#ab133737; RRID: AB_2811263
Goat Anti-OTX2	R and D Systems	Cat#AF1979; RRID: AB_2157172
Mouse Anti-PV	Sigma-Aldrich	Cat#P3088; RRID: AB_477329
Rabbit Anti-TH	Millipore	Cat#AB152; RRID: AB_390204
Bacterial and Virus Strains		
Lentiviral particles expressing pBOB-hSYN-HTB	Previous publication (Grealish et al., 2015)	Addgene Cat#30195
EnvA-pseudotyped G-deleted mCherry rabies virus	Previous publication (Grealish et al., 2015)	N/A
Chemicals, Peptides, and Recombinant Proteins		
Cholera Toxin B Subunit (Choleragenoid) from *Vibrio cholerae* in Low Salt	List Biologicals	Cat#104
Experimental Models: Cell Lines		
RC-17 cell line	Roslin Cells	RRID: CVCL_L206
Experimental Models: Organisms/Strains		
Rat: Sprague-Dawley: Crl:CD(SD)	Charles River	RGD Cat#734476; RRID: RGD_734476
Rat: Athymic nude: Hsd:RH-Foxn1^{rnu}	Harlan / Envigo	RGD Cat#5508395; RRID: RGD_5508395
Oligonucleotides		
qPCR primers	Integrated DNA Technologies	(See Table S1 for sequences)
Software and Algorithms		
ImageJ (Fiji) Version 2.0.0-rc69/1.52i	Schindelin et al., 2012	https://imagej.net/Fiji#Downloads
Ridge detection ImageJ plugin	Steger, 1998	https://imagej.net/Ridge_Detection

LEAD CONTACT AND MATERIALS AVAILABILITY

Further information and requests for resources and reagents should be directed to and will be fulfilled by the Lead Contact, Malin Parmar (malin.parmar@med.lu.se). This study did not generate new unique reagents.

EXPERIMENTAL MODEL AND SUBJECT DETAILS

hESC differentiation and transgene expression

RC-17 ESCs (Roslin Cells, human female, passage 28) expressing the rabies helper construct (generated by lentiviral infection as described in Cardoso et al. (2018) cultured at 37°C and 5% CO_2 were used for all transplantation experiments. Neural differentiation

and regional patterning toward a VM fate was performed via dual SMAD inhibition to induce neuralization, GSK3 inhibitor-mediated caudalization, and SHH-mediated ventralization, as described in detail in Nolbrant et al. (2017). Cells were patterned toward a ventral FB fate according to the protocol detailed in Kirkeby et al. (2012).

Research animals

All procedures were performed in accordance with the European Union Directive (2010/63/EU), follow 3R principles, and were approved by the local ethical committee for the use of laboratory animals and the Swedish Department of Agriculture (Jordbruksverket). Adult female, athymic "nude" rats were purchased from Harlan/Envigo Laboratories (Hsd:RH-Foxn1rnu) and used to study the effect of graft placement and phenotype on fiber outgrowth and synaptic integration (n = 35). Adult (225–250 g) female Sprague–Dawley rats were purchased from Charles River and used to study the impact of nigrostriatal lesion on synaptic integration (n = 18), and for nigral CTB tracing (n = 2) and tissue clearing / light sheet microscopy (n = 3). Female host animals were used exclusively to enable long-term cohabitation in the cage size available in our vivarium, and as such our study does not assess the influence of host sex. Athymic "nude" rats were housed together in ventilated cages with *ad libitum* access to food and water, under a 12-hr light/dark cycle. Sprague-Dawley rats were housed as described above but in standard caging. Endpoints of this study were predetermined by design or by adherence to ethical permit.

METHOD DETAILS

Study design

Graft placement and phenotype comparisons

Adult female, athymic "nude" rats were used to study the effect of graft placement and phenotype on fiber outgrowth and synaptic integration (Figures 1, 2, 3, 4, and 5, excluding tissue clearing and light sheet imaging depicted in Figures 2I and 3I). Upon reaching an adult weight of approximately 225 g, the rats were lesioned by injection of 6-OHDA to the medial forebrain bundle (see below for details). Lesion severity was measured 4 weeks later by amphetamine-induced rotations (intraperitoneal injection of 2.5 mg/kg of amphetamine; Apoteksbolaget, Sweden) and recorded over 90 min using an automated system (Omnitech Electronics). After this, animals were grafted to the striatum or the nigra with FB- or VM-patterned progenitors. Only the animals with surviving grafts that were discretely placed within the midbrain or striatum were analyzed: intrastriatal grafting of VM-patterned progenitors (n = 7); intrastriatal grafting of FB-patterned progenitors (n = 5); intranigral grafting of VM-patterned progenitors (n = 5); intranigral grafting of FB-patterned progenitors (n = 6). 23 weeks post-transplantation, "nude" rats received an injection of EnvA-pseudotyped ΔG mCherry rabies to the graft site and were perfused 7 days later. Fiber outgrowth from animals with 24-week VM-patterned grafts to the substantia nigra (n = 5) is described in Cardoso et al. (2018). In this study, we have used data from the same animals to generate the schematic in Figure 2A, which is included here to provide the comparison to the new data for FB-patterned intranigral, and VM- and FB-patterned intrastriatal graft fiber outgrowth as shown in Figures 2B, 3A, and 3B. The imaging (Figures 2C–2F and 3C–3F) used to produce hNCAM fiber counts (Figures 2J and 3L) was newly performed for all animals in this study.

Tissue clearing and nigral CTB tracing

Adult (225–250 g) female Sprague–Dawley rats (n = 5) received righthand VTA and MFB lesions as detailed below. Amphetamine-induced rotations as described above was used to determine lesion efficiency. Animals were transplanted with VM-patterned progenitors to the striatum, for tissue clearing and light sheet microscopy (Figures 2I and 3I, n = 3) or simultaneous rabies / CTB tracing (Figure 6, n = 2), after 16 or 13 weeks of graft maturation plus 1 week of rabies / CTB tracing, respectively. Rats were immunosuppressed with daily injections of cyclosporine (10 mg/kg/day, intraperitoneally; Apoteksbolaget, Sweden), starting 2 days prior to transplantation, until the end of the experiment, to prevent graft rejection.

Lesioned and intact host comparisons

Adult (225–250 g) female Sprague–Dawley rats (n = 18) were purchased from Charles River and used to study the impact of nigrostriatal lesion on synaptic integration (Figure 7). Ten of the animals received an injection of 6-OHDA to the medial forebrain bundle (as detailed below), whereas eight were kept intact. 17 weeks after lesion, and following amphetamine-induced rotations to determine lesion efficiency, all rats were transplanted with VM-patterned progenitors to the striatum. 6 weeks later, animals received an injection of EnvA-pseudotyped ΔG mCherry rabies to the graft site and were perfused 7 days later. Only animals with surviving grafts that were discretely placed within the striatum were analyzed subsequently (n = 5 lesioned, n = 5 intact). Parafascicular nucleus, external globus pallidus, and cortex were selected *a priori* for quantification because of their consistent labeling in previous experiments. Rats were immunosuppressed with daily injections of cyclosporine (10 mg/kg/day, intraperitoneally; Apoteksbolaget, Sweden), starting 2 days prior to transplantation, until the end of the experiment, to prevent graft rejection.

ΔG-rabies production

EnvA-pseudotyped ΔG-rabies was produced as described in Grealish et al. (2015). Titers were 20–30 × 10^6 TU/ml and a working dilution of 5% was used for injection *in vivo*.

Surgical procedures

Graft placement and phenotype comparisons

All surgical procedures were performed under general anesthesia using a solution of fentanyl and medetomidine (20:1) injected intraperitoneally (1 mL/kg; Apoteksbolaget, Sweden). Lesion of the nigrostriatal pathway in nude rats was induced by unilateral injection of 6-hydroxydopamine into the right MFB, with a volume of 4 μL at freebase concentration of 3.5 μg/μL to the following coordinates relative to bregma: A/P −4; M/L −1.2; D/V (from dura) −7.5.

Four weeks after 6-OHDA MFB lesion, "nude" rats received a total dose of either 150,000 or 75,000 hESC-derived progenitors at day 16 of differentiation into the striatum or substantia nigra respectively. A volume of 2 μL, at a concentration 75,000 cells/μL at a rate of 1 μL per minute and diffusion time of 2 min was transplanted to striatum at the following coordinates relative to bregma: A/P +0.5; M/L −3; D/V (from dura) −4.5; adjusted to flat head. A volume of 2 μL, at a concentration 37,500 cells/μL at a rate of 1 μL per minute and diffusion time of 2 min was transplanted to the substantia nigra at the following coordinates relative to bregma: A/P −5.2; M/L −2.3; D/V (from dura) −7; adjusted to flat head.

EnvA-pseudotyped ΔG mCherry rabies virus at a dilution of 5% of the stock was injected at a rate of 0.5 μL per minute and diffusion time of 2 min at the transplantation site. A total volume of 4 μL was injected into the striatum at 2 sites at a volume of 2 μL per site to the following coordinates relative to bregma: 1) A/P +0.5; M/L −3.0; D/V (from dura) −5/-4. 2) A/P +0.5; M/L −2.5; D/V (from dura) −5/-4; adjusted to flat head. A volume of 2 μL was injected in substantia nigra to the following coordinates relative to bregma: A/P −5.2; M/L −2.3; D/V (from dura) −7; adjusted to flat head. Animals were perfused 1 week after rabies injection.

Tissue clearing and nigral CTB tracing

Lesion of the nigrostriatal pathway and VTA in Sprague-Dawley rats used for tissue clearing and light sheet microscopy or simultaneous rabies / CTB tracing received lesions was induced by unilateral injection of 6-hydroxydopamine with a volume of 3.0 μL and 2.5 μL at freebase concentration of 3.5 μg/μL to the following coordinates relative to bregma: A/P −4.4; M/L −1.2; D/V (from dura) −7.8; and A/P −4.0; M/L −0.8; D/V (from dura) −8.0, adjusted to flat head, respectively. Rats were grafted with 150,000 VM-patterned progenitors in two deposits to the striatum at a total volume of 2 μL, at a concentration of 75,000 cells/μL, at a rate of 1 μL per minute and diffusion time of 2 min, to the following coordinates relative to bregma: A/P +0.5; M/L −2.6; D/V (from dura) −4.0/-3.5; adjusted to flat head. Animals grafted in the nigra received 75,000 cells in a total volume of 1 μL to the following coordinates relative to bregma: A/P −5.2; M/L –2.3; D/V (from dura) –7.0; adjusted to flat head. For rabies / CTB tracing, animals first received two 500 nL nigral CTB (choleragenoid in low salt, List Biological Laboratories, 0.4% in PBS) injections at A/P −5.3; M/L −1.6, −2.6; D/V −7.2, −6.7 (from dura); adjusted to flat head relative to bregma, at a rate of 100 nL/min and a diffusion time of 3 minutes, followed by a total volume of 2 μL ΔG-rabies at a dilution of 5% of the stock injected at a rate of 0.5 μL per minute and diffusion time of 2 min to the following coordinates relative to bregma: A/P +0.5; M/L −2.6; D/V (from dura) −4.0/-3.5; adjusted to flat head. Animals were perfused after 1 week of rabies / CTB tracing.

Lesioned and intact host comparisons

Lesion of the nigrostriatal pathway in Sprague-Dawley rats used in the intact versus lesion experiment was induced by unilateral injection of 6-hydroxydopamine into the right MFB, with a volume of 3 μL at freebase concentration of 3.5 μg/μL to the following coordinates relative to bregma: A/P −4.4; M/L −1.1; D/V (from dura) −7.8, adjusted to flat head. Rats received 300,000 cells into two deposits in striatum, at a total volume of 4 μL, at a concentration 75,000 cells/μL, at a rate of 1 μL per minute and diffusion time of 2 min to the following coordinates relative to bregma: A/P +1.0; M/L −2.6; D/V (from dura) −4.5/-3.5; adjusted to flat head. A total volume of 2 μL ΔG-rabies at a dilution of 5% of the stock was injected at a rate of 0.5 μL per minute and diffusion time of 2 min to the following coordinates relative to bregma: A/P +1.0; M/L −2.6; D/V (from dura) −4.5/-3.5; adjusted to flat head. Animals were perfused 1 week after rabies injection.

Tissue clearing

Brains with VM-patterned grafts in either the nigra or the striatum were processed for light sheet microscopy using the iDISCO clearing method (Renier et al., 2014). Following perfusion with 2% PFA, the brains were post-fixed on ice for 1 hour, then stored in PBS before being divided by a midline sagittal cut, with each half-brain processed individually. The samples were: Washed in PBS 3x 30 min, then in 20, 40, 60 and 80% methanol (in PBS), and 100% methanol, for 1 hour each. Incubated in DCM-methanol (2:1) overnight at room temperature with shaking, followed by 2x 30 min wash in 100% methanol and 1 hour at 4°C. Bleached in 5% H_2O_2, shaking overnight at 4°C. Rehydrated from methanol to 20, 40, 60, 80, 100% PBS, 30 min in each step. Washed in PBS/2% TritonX (PTx.2) 2x 1 hour at room temperature, followed by a wash in PBS/0.2% Tween-20 with 10 μg/ml heparin (PTwH) 2x 30 min. Incubated in permeabilization buffer (PTx.2/glycine/DMSO) at 37°C for 3-5 days, with shaking. Washed 2x 30min in PTx.2, then incubated with primary antibody in PTwH, 5% DMSO/3% Serum (NDS) at 37°C for 10 days: rabbit polyclonal anti-TH (Millipore) at 1:1000 and mouse monoclonal anti-hNCAM (Santa Cruz) at 1:1000. Washed in PTwH 10, 15, 20 min, then every hour during the day. Incubated at 37°C with donkey Alexa Fluor 647-conjugated secondary antibodies in PTwH/3% normal donkey serum (NDS) for 10 days. Washed in PTwH 10, 15, 20 min, then every hour during the day, and left overnight. Dehydrated to 20, 40, 60, 80, then 100% methanol, 1 hour in each step, followed by 100% methanol overnight. Incubated in DCM-methanol (6+4) with shaking overnight. Incubated in 100% DCM 15 min twice, then changed to DiBenzyl Ether (DBE) for clearing. All solutions were filtered before use and 0.02% NaN3 was added to all stock solutions to prevent microbial growth.

Light sheet microscopy

The cleared hemi-brains were imaged on an Ultra Microscope II (LaVision Biotec) equipped with an sCMOS camera (Andor Neo, model 5.5-CL3) and 4x or 12x objective lenses (LaVision LVMI-Fluor 4x/0.3 or 12x/0.53 MI Plan). We used two laser configurations with following emission filters: 525/50 for endogenous background and AlexaFluor 488, and 680/30 for AlexaFluor 647. Stacks were acquired with ImspectorPro64 (LaVision Biotec) using 5 μm z-steps. Samples were imaged in a chamber filled with DBE. Several stacks (mosaic acquisition) were taken with 10% overlap to cover a hemi-brain. These image stacks were stitched to visualize the brain in 3D with Arivis Vision 4D 3.01 (Arivis AG). Rendered movies were compiled in Final Cut Pro 10.4.3 (Apple Inc.).

Immunohistochemistry

Prior to perfusion, rats were given terminal anesthesia with a lethal dose of 60 mg/kg sodium pentobarbitone injected intraperitoneally (Apoteksbolaget, Sweden). The animals were transcardially perfused with physiological saline solution followed by ice-cold 4% paraformaldehyde. Brains were post-fixed for 2 h in 4% paraformaldehyde, transferred to 25% sucrose for 48 hr and sectioned at a 35 μm thickness (1:8 series) using a freezing microtome. For DAB-developed immunohistochemistry, free floating sections were incubated with Tris-EDTA pH 9.0 for 15 minutes at 80°C for antigen retrieval. Immunohistochemistry was performed on free floating sections that were incubated with primary antibodies overnight in 0.1 M KPBS solution containing 0.25% Triton-X and 5% serum for the species specific to the secondary antibody. Sections were then incubated with fluorophore-conjugated (fluorescent detection) or biotin-coupled (DAB detection) secondary antibodies for 1 hr in the same solution. All stained sections were mounted on gelatin-coated microscope slides. Fluorescent sections were coverslipped using polyvinyl alcohol mounting medium with DABCO (Sigma-Aldrich). DAB-developed sections were dehydrated in an ascending series of alcohols, cleared with xylene, coverslipped using DPX mountant and left to dry overnight.

A biotinylated tyramide signal amplification (TSA) protocol (Adams, 1992) was used to boost fluorescent detection of FOXA2, μ-opioid receptor (MOR), and hNCAM (in Figures 2 and 3): After labeling with primary antibody, sections were incubated in biotinylated secondary antibodies for 1 hr at room temperature, washed, and then incubated with ABC solution for 30 min. Sections were washed, then incubated with biotinyl tyramide (1:2500 in KPBS containing 0.009% H2O2) for 30 min. A second round of TSA amplification was used for Figures 2G, 2H and 2K. Sections were then fluorescently labeled by 2 hr incubation with fluorophore-conjugated streptavidin (1:500). Finally, sections were washed and mounted as described above.

Primary antibodies were used as follows:

Goat anti-CTB (1:2500; List Biological Laboratories); rabbit anti-CTIP2 (1:1000; Abcam ab28448); rabbit anti-DARPP-32 (1:250 Cell Signaling 2306); goat anti-FOXA2 (1:500; Santa Cruz Biotechnology sc-6554); rabbit anti-FOXG1 (1:200; Abcam ab18259); mouse anti-FOXP2 (1:500; Millipore MABE415); chicken anti-GFP (1:1000; Abcam ab13970); mouse anti-hNCAM (1:1000; Santa Cruz Biotechnology sc-106); mouse anti-HuNu (1:200; Millipore MAB1281); goat anti-mCherry (1:1000; SICGEN AB0040-200); rabbit anti-mCherry (1:1000; Abcam ab167453); guinea pig anti-MOR (1:1000; Millipore ab5509); rabbit anti-NKX2.1 (aka TTF1; 1:250; Abcam ab133737) mouse anti-parvalbumin (1:2000; Sigma-Aldrich P3088); rabbit anti-TH (1:1000; Millipore AB152).

Immunocytochemistry

For immunocytochemistry cells were blocked in 0.1M KPBS containing 0.1% Trixon-X and 5% serum matching the secondary antibodies for 1-3 hours. Cells were incubated with primary antibodies overnight at 4°C in blocking solution, washed, and incubated with fluorescent secondary antibodies for 2 hours at room temperature. Primary antibodies were used as follows: LMX1A/B (1:1000; Millipore AB10533), OTX2 (1:2000; R&D AF1979), FOXA2 (1:500; Santa Cruz Biotechnology sc-6554), NKX2.1 (aka TTF1; 1:500; Abcam ab133737).

qRT-PCR

RNA was extracted from cells with the RNeasy Micro kit (QIAGEN). Reverse transcription was performed with the Maxima First Strand cDNA Synthesis Kit for RT-qPCR (Thermo Fisher Scientific). cDNA was prepared with LightCycler 480 SYBR Green I Master mix (Roche) using the Bravo instrument (Agilent) and analyzed on a LightCycler 480 instrument using a 2-step protocol with a 60°C annealing/elongation step. All samples were run in technical triplicates, and the average Ct-values were used for calculations. Data are represented using the DDCt method. All fold changes are calculated as the average fold change based on 2 different housekeeping genes (*ACTB* and *GAPDH*). The primers used are described in Table S1 (Integrated DNA Technologies).

Microscopy and image analysis

All brightfield images were captured using a Leica microscope equipped with an external camera, while fluorescent images were acquired using a TCS SP8 laser scanning confocal microscope. Quantitative comparisons were performed on image sets collected under the same imaging and acquisition conditions. Quantification of the percentage of host inputs by structure (Figure 4) was based on the anatomical location of $mCherry^+$ neurons in accordance with the matching coronal section from the Paxinos and Watson rat brain atlas (Paxinos and Watson, 2005).

For representation of graft derived fiber outgrowth an entire 1:8 series of hNCAM DAB-stained sections were scanned and images were placed against the matching coronal section from the Paxinos and Watson rat brain atlas (Paxinos and Watson, 2005). The area covered by $hNCAM^+$ outgrowth was then mapped onto each anatomical plane. For the representation of host synaptic inputs to the

graft, the same process was done with mCherry DAB-stained sections, with each dot representing the location of an $mCherry^+$ neuron.

Quantification of total inputs and percentage of inputs in intact versus lesioned animals (Figure 7) was done by blinded manual counting with an Olympus AX70 fluorescent microscope. $hNCAM^+$ fiber count density (Figures 2J and 3L) was generated from 185 μm x 185 μm confocal stacks of 35 μm thick DAB-developed sagittal sections, using an ImageJ (Fiji) (Schindelin et al., 2012) macro applied equally to all images that: detected ridges (Steger, 1998), converted detected axons to binary images, and counted individual axons entering the imaged volume from each edge. TH^+hNCAM^+ fiber quantification in host dlSTR for intranigral grafts was performed manually by a blinded counter following automated thresholding and channel overlap using an ImageJ macro applied equally to all images (Figure 2K). PV^+ neuron counts (Figures 7K and 7L) were performed by automated image analysis applied equally to images from the GPe of all animals (Figures 7G and 7H) using an ImageJ (Fiji) macro that applied: Gaussian blur, an automatic local threshold, a watershed algorithm to segment adjacent cells, particle detection to exclude small subcellular fragments, and automatic detection and counting of overlapping objects among the NeuN, rabies, and PV channels. Starter neuron quantification (Figure S2) was performed manually with ImageJ by first marking $Rabies^+GFP^+$ neurons in confocal stacks, before revealing the TH channel.

QUANTIFICATION AND STATISTICAL ANALYSIS

The details of each quantitative comparison made can be found here and in the associated Figure Legends. Animals excluded on the basis of absent or misplaced grafts were removed before statistical testing. All mean values represent the average of all experimental animals analyzed. Statistically analyzed comparisons were generated by a blinded counter, or automated image analysis applied equally to all images collected. Figures 2J, 3L, 7E, 7K, and 7L were analyzed by two-way ANOVA with Bonferroni-corrected post hoc testing, with $p < 0.05$ considered significant ($\alpha = 0.05$). Figures 2K and 7F were analyzed by unpaired two-tailed t test, with $p < 0.05$ considered significant. Data are presented as means ± SEM.

DATA AND CODE AVAILABILITY

This study did not generate new datasets or code.

Cell Reports, Volume *28*

Supplemental Information

hESC-Derived Dopaminergic Transplants Integrate into Basal Ganglia Circuitry in a Preclinical Model of Parkinson's Disease

Andrew F. Adler, Tiago Cardoso, Sara Nolbrant, Bengt Mattsson, Deirdre B. Hoban, Ulla Jarl, Jenny Nelander Wahlestedt, Shane Grealish, Anders Björklund, and Malin Parmar

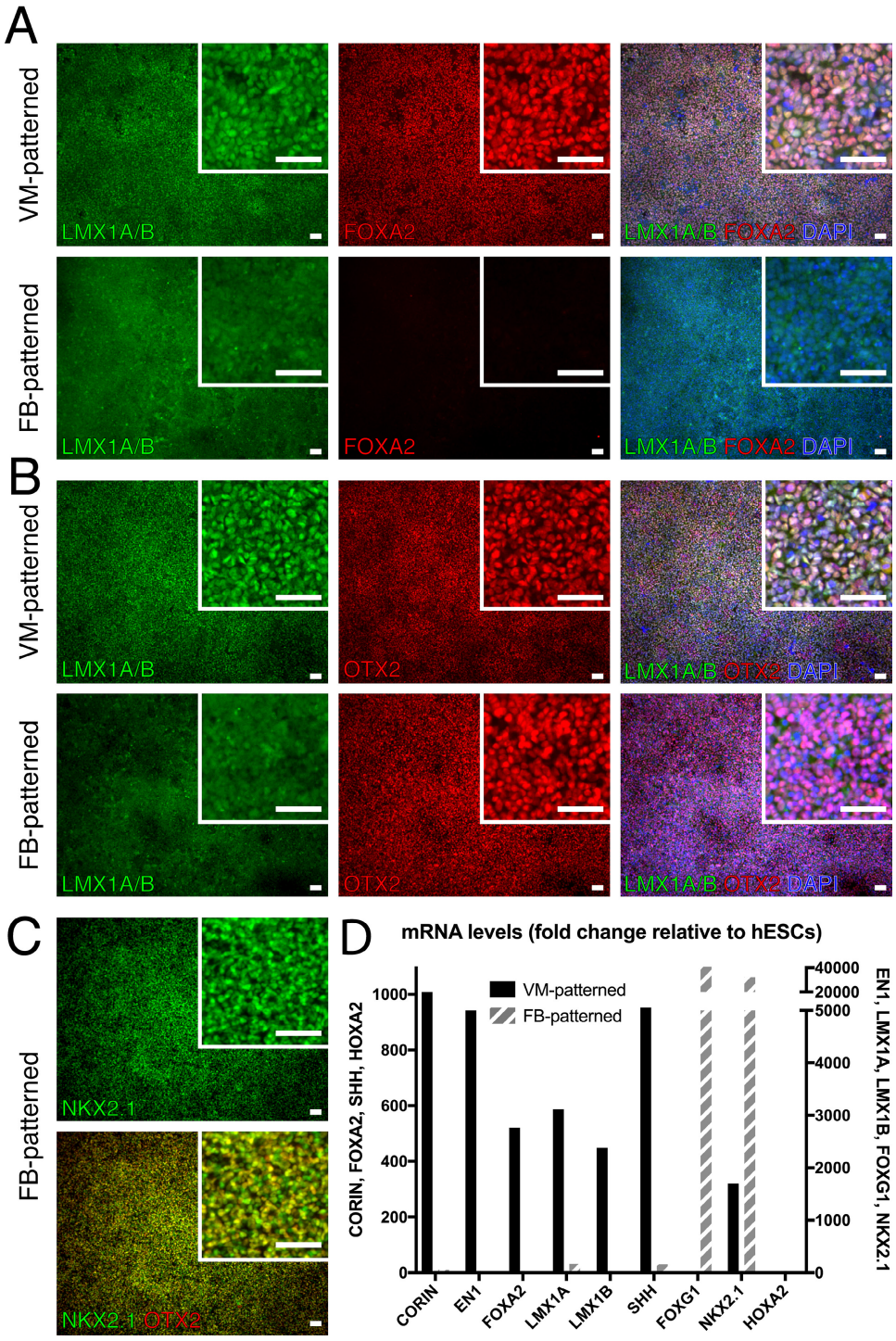

Figure S1. *In vitro* characterization of ventral midbrain- and ventral forebrain-patterned cell grafts (related to Fig. 1)

(A) At day 14 of differentiation, hESC-derived VM-patterned progenitors co-expressed ventral midbrain markers LMX1A/B and FOXA2, while FB-patterned progenitors did not, and **(B)** both cell sources expressed the anterior marker OTX2. **(C)** At day 21 of differentiation, FB-patterned progenitors expressed the ventral forebrain marker NKX2.1. **(D)** qPCR analysis at day 14 of differentiation (two days before grafting) revealed VM- and FB-patterned cells adopted ventral midbrain and ventral forebrain fates, respectively, without expression of the hindbrain marker *HOXA2*.

Scale bars represent 100 µm. DAPI = 4′,6-diamidino-2-phenylindole; EN1 = homeobox protein engrailed-1; FB = forebrain; FOXA2 = forkhead box A2; HOXA2 = homeobox A2; LMX1A/B = LIM homeobox transcription factor 1 alpha/beta; NKX2.1 = NK2 homeobox 1; OTX2 = orthodenticle homeobox 2; SHH = sonic hedgehog; VM = ventral midbrain

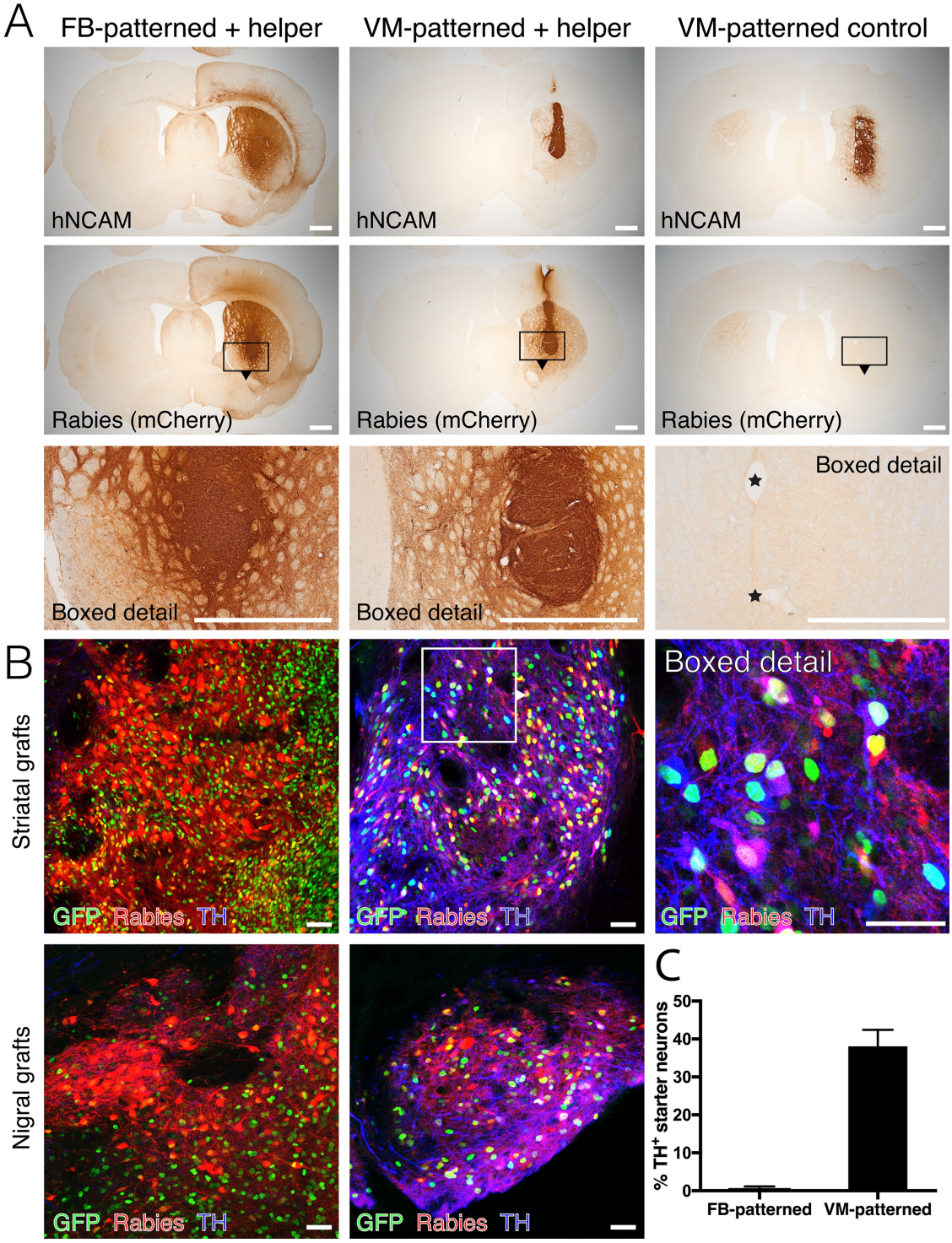

Figure S2. EnvA-pseudotyped ΔG-rabies tracing starter cell characterization (related to Fig. 4)
(A) hNCAM and ΔG-rabies (mCherry) staining reveals both FB- and VM-patterned progenitor cells generate neuron-rich grafts, but only animals grafted with cells pre-transduced with the rabies helper construct express mCherry upon injection of EnvA-pseudotyped mCherry ΔG-rabies virus. Stars indicate rabies injection sites for a 6 week VM-patterned control graft. **(B)** Analysis of intrastriatal and intranigral graft-derived "starter" cells, expressing both mCherry (ΔG-rabies) and nuclear GFP (rabies helper construct), reveals that **(C)** 38 ± 4.3 % of VM-patterned starter neurons were TH^+ (mean + SEM, VM-patterned grafts, n = 8 animals; FB-patterned grafts, n = 11 animals).

Scale bars represent 1 mm (A), 50 µm (B). FB = forebrain; GFP = green fluorescent protein; hNCAM = human neural cell adhesion molecule; TH = tyrosine hydroxylase; VM = ventral midbrain

	Forward	Reverse
ACTB	CCTTGCACATGCCGGAG	GCACAGAGCCTCGCCTT
CORIN	CATATCTCCATCGCCTCAGTTG	GGCAGGAGTCCATGACTGT
EN1	CGTGGCTTACTCCCCATTTA	TCTCGCTGTCTCTCCCTCTC
FOXA2	CCGTTCTCCATCAACAACCT	GGGGTAGTGCATCACCTGTT
FOXG1	TGGCCCATGTCGCCCTTCCT	GCCGACGTGGTGCCGTTGTA
GAPDH	TTGAGGTCAATGAAGGGGTC	GAAGGTGAAGGTCGGAGTCA
HOXA2	CGTCGCTCGCTGAGTGCCTG	TGTCGAGTGTGAAAGCGTCGAGG
LMX1A	CGCATCGTTTCTTCTCCTCT	CAGACAGACTTGGGGCTCAC
LMX1B	CTTAACCAGCCTCAGCGACT	TCAGGAGGCGAAGTAGGAAC
NKX2.1	AGGGCGGGGCACAGATTGGA	GCTGGCAGAGTGTGCCCAGA
SHH	CCAATTACAACCCCGACATC	AGTTTCACTCCTGGCCACTG

Table S1. Primer sequences (related to STAR Methods)